iScience

CellPress
OPEN ACCESS

Article

The HRD1-SEL1L ubiquitin ligase regulates stress granule homeostasis in couple with distinctive signaling branches of ER stress

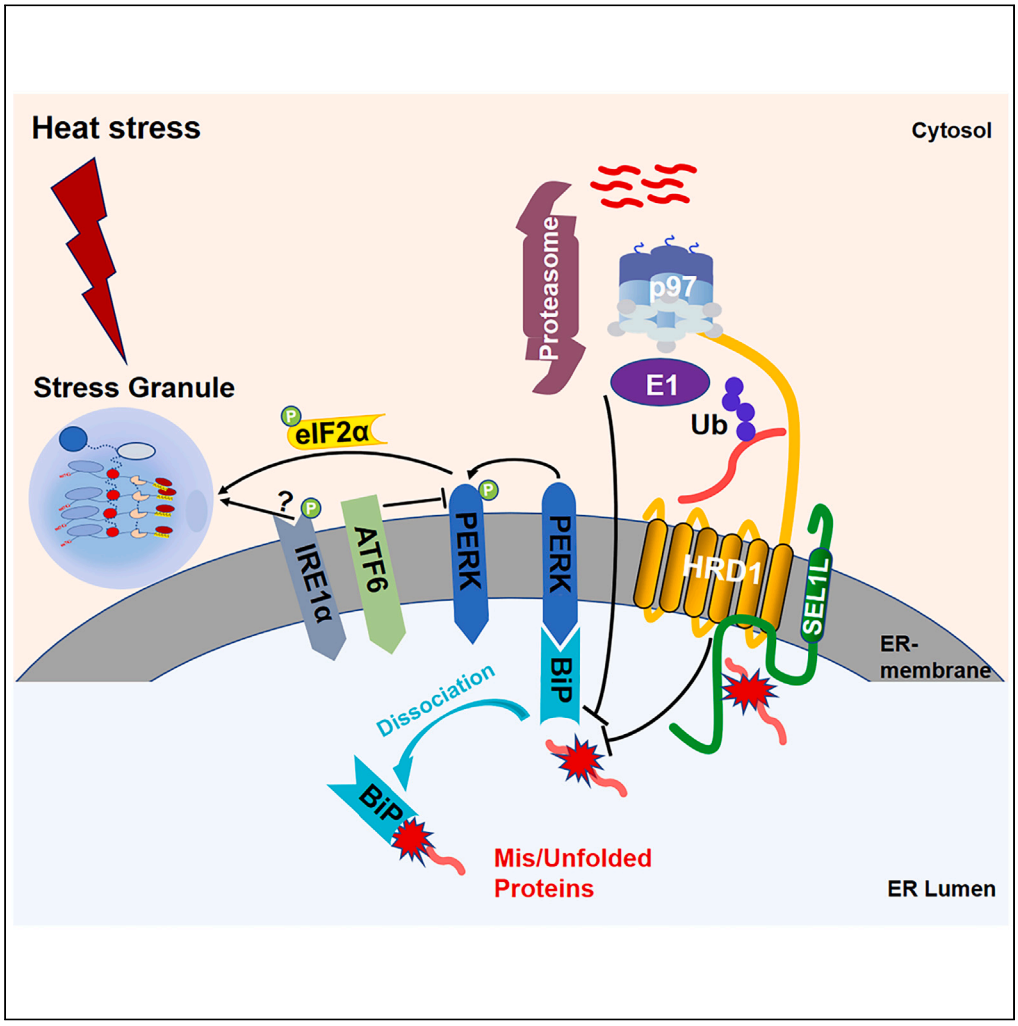

Wenbo Shi, Ran Ding, Yilin Chen, Fubo Ji, Junfang Ji, Weirui Ma, Jianping Jin

jianping_jin@zju.edu.cn

Highlights

HRD1-SEL1L ubiquitin ligase regulates heat shock-induced SG homeostasis specifically

Distinct ER stress branches play differential roles in SG homeostasis

The HRD1-SEL1L complex mediates SG homeostasis via the BiP-PERK-eIF2α signaling axis

Shi et al., iScience 27, 110196
July 19, 2024
https://doi.org/10.1016/j.isci.2024.110196

iScience

CellPress
OPEN ACCESS

Article

The HRD1-SEL1L ubiquitin ligase regulates stress granule homeostasis in couple with distinctive signaling branches of ER stress

Wenbo Shi,[1] Ran Ding,[1] Yilin Chen,[1] Fubo Ji,[1] Junfang Ji,[1,2,3] Weirui Ma,[1] and Jianping Jin[1,2,3,4,*]

SUMMARY

Stress granules (SGs) are membrane-less cellular compartments which are dynamically assembled via biomolecular condensation mechanism when eukaryotic cells encounter environmental stresses. SGs are important for gene expression and cell fate regulation. Dysregulation of SG homeostasis has been linked to human neurodegenerative disorders, including amyotrophic lateral sclerosis (ALS) and frontotemporal dementia (FTD). Here we report that the HRD1-SEL1L ubiquitin ligase complex specifically regulates the homeostasis of heat shock-induced SGs through the ubiquitin-proteasome system (UPS) and the UPS-associated ATPase p97. Mechanistically, the HRD1-SEL1L complex mediates SG homeostasis through the BiP-coupled PERK-eIF2α signaling axis of endoplasmic reticulum (ER) stress, thereby coordinating the unfolded protein response (UPR) with SG dynamics. Furthermore, we show that the distinctive branches of ER stress play differential roles in SG homeostasis. Our study indicates that the UPS and the UPR together via the HRD1-SEL1L ubiquitin ligase to maintain SG homeostasis in a stressor-dependent manner.

INTRODUCTION

Stress granules (SGs) are non-membranous organelles arising when eukaryotic cells undergo various stress conditions like heat shock, oxidative stress, UV irradiation, or viral infection etc.[1–3] SGs mainly consist of exposed mRNA, the 40S ribosomal subunit, and dozens of RNA-binding proteins (RBPs) including G3BP1/2, hnRNPs, and TIA-1/R which constitute the core of SGs.[4–7] These messenger ribonucleoprotein complexes (mRNPs) subsequently oligomerize and recruit various shell proteins and regulatory proteins through biomolecular condensation driven by a multivalent interaction network involving RNA-RNA, protein-protein, and RNA-protein interactions.[7–9] SGs are assembled transiently and harbor the pre-initiation complexes of translation which is inactivated to prevent production of damaged or misfolded protein during stress conditions, while allowing the timely resumption of translation initiation upon stress relief.[10–12] The highly dynamic SGs can function as temporary "shelters" ensuring proper RNA metabolism, protein translation and cytosolic proteostasis during stress responses.[13] Furthermore, aberrant SG homeostasis has been implicated in the pathogenesis of several neurodegenerative disorders such as amyotrophic lateral sclerosis (ALS) and frontotemporal dementia (FTD).[14,15] Therefore, therapeutically targeting SG homeostasis could potentially provide avenues for curbing pathogenesis of these neurodegenerative disorders.

The crucial roles of post-translational modifications (PTMs) such as phosphorylation,[16–18] poly (ADP)ribosylation,[19] methylation,[20] along with their respective signaling pathways, started to be uncovered for regulating SG homeostasis. For example, phosphorylation of the α subunit of eukaryotic translation initiation factor 2 (eIF2α) at its serine-51 site is a crucial signal that triggers the assembly of SGs upon various stimuli.[5,21] Five upstream kinases including PKR, PERK, GCN2, FAM69C, and HRI have been reported to mediate the phosphorylation of mammalian eIF2α under distinctive stress conditions.[22–27] However, upstream pathways leading to these phosphorylation cascades are still unclear.

Protein ubiquitination is one of the most important PTMs and is critical for various signaling events including cellular proteostasis in eukaryotes.[28] Ubiquitination is catalyzed by an enzymatic cascade of E1-E2-E3 in which E3, i.e., ubiquitin ligase, governs substrate specificity.[29,30] Thus far, over 600 ubiquitin ligases have been identified in human genome, but only three of them have been implicated in regulation of SG dynamics. Keiten-Schmitz et al. found that RNF4, a SUMO-targeted ubiquitin ligase, regulates SG homeostasis through clearance of the nuclear misfolded subfractions RBPs, such as TDP43, FUS, and hnRNPs.[31] This process could alleviate proteotoxic stress in the nucleus and facilitate cytoplasmic SG resolution.[31] In another study, Valdez-Sinon et al. reported that inhibition of the anaphase promoting complex/cyclosome (APC/C) ubiquitin ligase and its regulatory subunit Cdh1 promotes the arsenite-induced SG formation in primary cortical neurons via an FMRP (Fragile X mental

[1]Life Sciences Institute, Zhejiang University, Hangzhou 310058, China
[2]Center for Life Sciences, Shaoxing Institute, Zhejiang University, Shaoxing 321000, China
[3]Cancer Center, Zhejiang University, Hangzhou 310058, China
[4]Lead contact
*Correspondence: jianping_jin@zju.edu.cn
https://doi.org/10.1016/j.isci.2024.110196

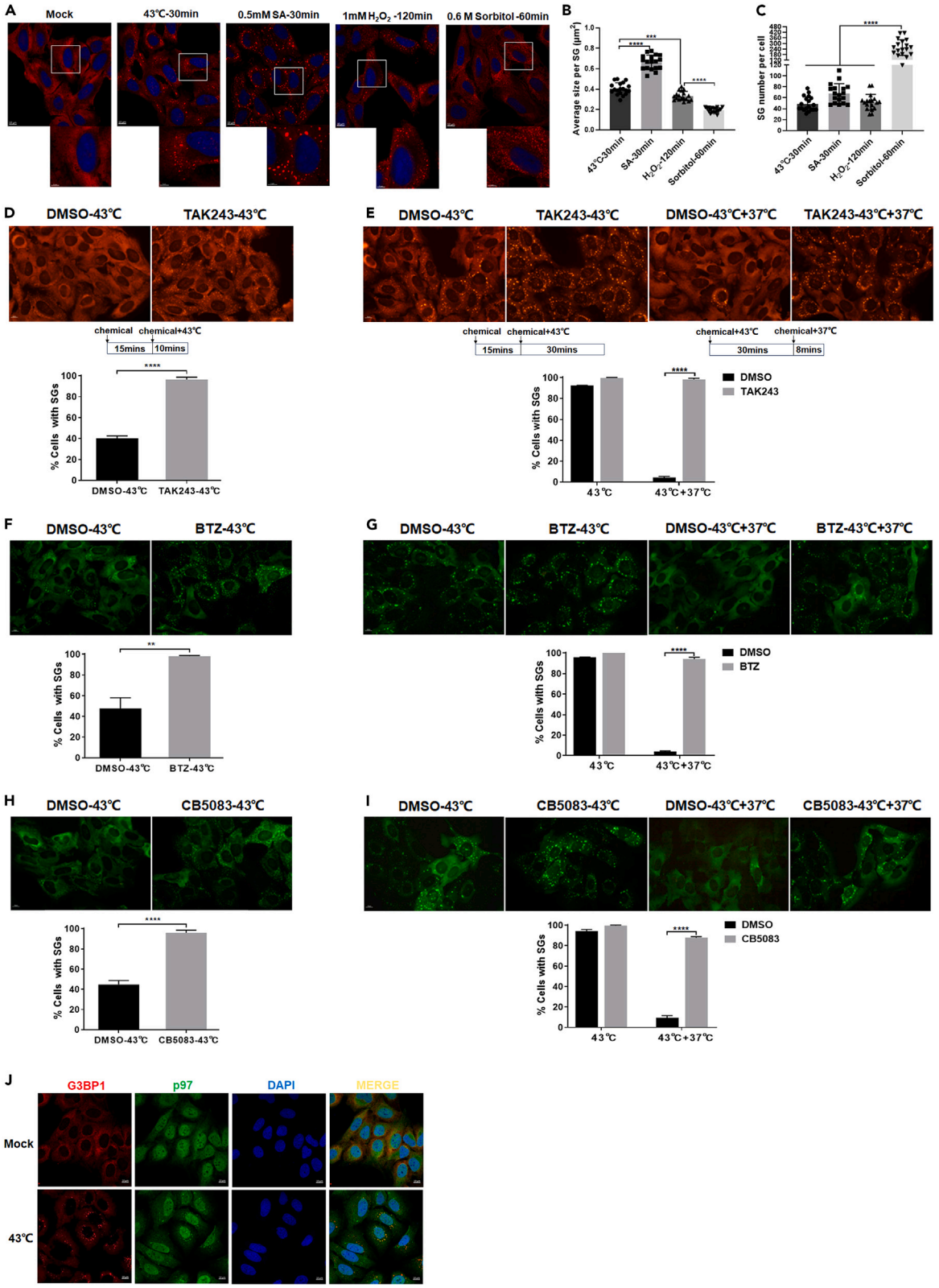
A
Mock
43℃-30min
0.5mM SA-30min
1mM H2O2 -120min
0.6 M Sorbitol -60min
B
Average size per SG (μm²)
43℃-30min
SA-30min
H2O2-120min
Sorbitol-60min
C
SG number per cell
43℃-30min
SA-30min
H2O2-120min
Sorbitol-60min
D
DMSO-43℃
TAK243-43℃
chemical
chemical+43℃
15mins
10mins
% Cells with SGs
DMSO-43℃
TAK243-43℃
E
DMSO-43℃
TAK243-43℃
DMSO-43℃+37℃
TAK243-43℃+37℃
chemical
chemical+43℃
15mins
30mins
chemical+43℃
chemical+37℃
30mins
8mins
% Cells with SGs
DMSO
TAK243
43℃
43℃+37℃
F
DMSO-43℃
BTZ-43℃
% Cells with SGs
DMSO-43℃
BTZ-43℃
G
DMSO-43℃
BTZ-43℃
DMSO-43℃+37℃
BTZ-43℃+37℃
% Cells with SGs
DMSO
BTZ
43℃
43℃+37℃
H
DMSO-43℃
CB5083-43℃
% Cells with SGs
DMSO-43℃
CB5083-43℃
I
DMSO-43℃
CB5083-43℃
DMSO-43℃+37℃
CB5083-43℃+37℃
% Cells with SGs
DMSO
CB5083
43℃
43℃+37℃
J
G3BP1
p97
DAPI
MERGE
Mock
43℃

Figure 1. SG assembly and disassembly are highly dynamic and regulated by the ubiquitin-proteasome system

In (D–I), upper and lower panels are representative images which were taken using microscope and their corresponding quantifications and statistical analysis, respectively. $n = 3$ replicates with >450 cells per condition.

(A) U2OS cells were cultured at 43°C for 30 min, or treated with 0.5 mM sodium arsenite (SA) for 30 min, 1 mM hydrogen peroxide (H_2O_2) for 2 h, and 0.6 M sorbitol for 1 h, respectively, and immunostaining was done using G3BP1 antibody. Scale bar: 10 μm.

(B and C) Quantification of average SG size (B), SG number per cell (C) from (A). Data are shown as mean ± SD, one-way ANOVA with Tukey's multiple comparisons test, ***$p \leq 0.001$; ****$p \leq 0.0001$, $n = 18$ with >160 cells and >5,000 SGs per condition.

(D) U2OS cells were pretreated using Uba1 inhibitor TAK243 for 15 min, and then cultured at 43°C for 10 min. Immunostaining was done using G3BP1 antibody. Data are shown as mean ± SD, unpaired two-tailed Student's t tests; ****$p \leq 0.0001$. Scale bar: 10 μm.

(E) U2OS cells were pretreated with TAK243 for 15 min and then cultured at 43°C for 30 min, or cells were treated at 43°C with TAK243 for 30 min followed by 37°C for 8 min. Immunostaining was done using G3BP1 antibody. Data are shown as mean ± SD, two-way ANOVA with Sidak's multiple comparisons test; ****$p \leq 0.0001$. Scale bar: 10 μm.

(F and H) The U2OS-EGFP-G3BP1 cells were pretreated using proteasome inhibitor Bortezomib (BTZ, F) or p97 inhibitor CB5083 (H) for 15 min, and then cultured at 43°C for 10 min. Data are shown as mean ± SD, unpaired two-tailed Student's t tests; **$p \leq 0.01$; ****$p \leq 0.0001$. Scale bar: 10 μm.

(G and I) The U2OS-EGFP-G3BP1 cells were pretreated with BTZ (G), or CB5083 (I) for 15 min and then cultured at 43°C for 30 min, or cells were treated at 43°C with BTZ (G), CB5083 (I) for 30 min followed by 37°C for 8 min. Data are shown as mean ± SD, two-way ANOVA with Sidak's multiple comparisons test; ****$p \leq 0.0001$. Scale bar: 10 μm.

(J) U2OS cells were cultured at 43°C for 30 min and immunostaining was done using G3BP1 and p97 antibodies. Scale bar:10 μm. See also Figure S1.

retardation protein)-dependent manner, although it remains unknown whether APC/C^{Cdh1} is responsible for ubiquitylating FMRP and how ubiquitylated-FMRP dampens SG formation in this scenario.[32] More recently, Yang et al. showed that the ubiquitin ligase TRIM21 localizes in SGs during oxidative stress.[33] In this case, TRIM21 mediates the K63-linked ubiquitination of the SG core protein G3BP1, leading to disruption of liquid-liquid phase separation (LLPS) and hence inhibiting SG formation under arsenite treatment.[33] Furthermore, other ubiquitination-related proteins have been implicated in regulating SG homeostasis as well. Gwon et al. proved that a ubiquitin-binding protein FAF2 recognizes polyubiquitylated G3BP1 and then extracts G3BP1 from heat shock-induced SGs to promote SG disassembly together with p97 (also called VCP, a valosin-containing protein), an ATPase and a ubiquitin-dependent segregase involving protein quality control and degradation.[34] In arsenite-induced SG homeostasis, Turakhiya et al. found that ZFAND1, a ubiquitin-like domain-containing protein, recruits p97 and the proteasome to stimulate the disassembly of SGs.[35] However, we are still at an early stage to fully understand the roles of ubiquitination, especially ubiquitin ligases in SG homeostasis. Considering that over 600 ubiquitin ligases exist in human protein network,[36] further studies are needed to uncover any other ubiquitin ligases which might also participate in regulating SG dynamics, as well as underlying mechanisms.

In this study, we systematically analyzed the roles of the ubiquitin-proteasome system (UPS) and found the UPS is important for SG homeostasis under distinct stress conditions. More significantly, we identified the HRD1-SEL1L ubiquitin ligase as a specific regulator of the heat shock induced-SG dynamics in a ubiquitination and p97-dependent manner. HRD1 and its cofactor, SEL1L form an *endoplasmic reticulum* (*ER*) membrane-residential RING finger ubiquitin ligase,[37] and constitute the core component of the ER-associated degradation (ERAD) machinery to mediate degradation of mis/unfolded ER proteins in the proteasome when dealing with ER stress.[38–40] Moreover, we showed that different signaling branches of ER stress possess differential effects on SG homeostasis, and the HRD1-SEL1L complex regulates SG homeostasis mainly through the ER stress-coupled Bip-PERK-eIF2α axis under the heat shock response.

RESULTS

SG assembly and disassembly are highly dynamic and regulated by the ubiquitin-proteasome system

To investigate the mechanisms by which SG assembly and disassembly are regulated under different stress conditions, we initially assessed the stress-induced formation of SGs labeled with G3BP1. Following exposure to various stressors, the endogenous G3BP1 proteins readily moved to SGs in U2OS cells (Figure 1A). While maintaining a generally rounded morphology, the size and quantity of SGs varied according to the particular stressor applied (Figures 1A–1C). SGs induced by heat shock or arsenite are large (Figures 1A and 1B). Conversely, SGs induced by H_2O_2 are relatively smaller in size (Figures 1A and 1B). We also noticed that sorbitol induced a higher quantity but much smaller SGs which were more evenly dispersed throughout the cytosol compared to SGs formed under other stress conditions (Figures 1A–1C). We next performed a time course experiment to investigate the assembly and disassembly kinetics of heat shock-induced SGs in U2OS and HeLa cells side by side. Interestingly, we observed that HeLa cells exhibit a faster formation of SGs in response to heat shock compared to U2OS cells. About 67% of HeLa cells already harbor SGs following exposure to 43°C for 10 min, in contrast to ~36% of U2OS cells (Figures S1A and S1B). Besides, the disassembly of SGs is also more rapid in HeLa than in U2OS cells. Merely ~10% of HeLa cells retain SGs upon recovery for 5 min, whereas ~31% of U2OS cells still harbor SGs (Figures S1A and S1B). These observations suggested that the kinetics of heat shock-induced SGs is also cellular context-dependent.

Next, we decided to determine whether the UPS has any differential effects on SG homeostasis under distinct stress conditions. Using immunostaining with antibodies of ubiquitin and G3BP1, we clearly showed that ubiquitin was strongly associated with G3BP1-labeled SGs upon the heat shock response (Figure S1C). Moreover, both K48- and K63-specific polyubiquitin conjugates were significantly increased upon heat shock, and these polyubiquitin chains were broken down rapidly as heat shock withdrew (Figure S1D).

To determine the effect of the UPS on the heat shock-induced SG homeostasis, we utilized small molecules that specifically target key components of the UPS machinery. For SG assembly, we incubated U2OS cells under 43°C for 10 min and observed SGs were formed

in ~40% cells (Figure 1D). TAK243, an inhibitor of ubiquitin E1 enzyme, Uba1, significantly promoted the assembly of heat shock-induced SGs, as SGs appeared in over 90% cells when TAK243 was applied (Figure 1D). For the disassembly, we cultured the U2OS cells under 43°C for 30 min to induce ~92.33% cells develop SGs, then dropped the temperature to 37°C for 8 min. In the control, only ~4.43% cells remained SGs. However, TAK243 almost totally blocked the SG disassembly (Figure 1E). In addition, we established a reporter cell line by expressing an EGFP-tagged G3BP1 in U2OS cells (referred to as U2OS-EGFP-G3BP1) (Figure S1E), and observed a similar effect of TAK243 on heat shock-induced SG homeostasis in the reporter cells (Figures S1F and S1G), implying that ubiquitination is important for the homeostasis of the heat shock-regulated SGs. Similar to the E1 inhibitor, bortezomib, an FDA-approved proteasome inhibitory drug, enhanced the assembly of the heat shock-stimulated SGs while impeding disassembly (Figures 1F and 1G). Together, these data suggested a substantial role of the UPS in regulating SG homeodynamics during the heat shock response.

To further prove the effect of the UPS on SG assembly and disassembly, we used CB5083 to block the activity of p97, an AAA family ATPase involving in protein degradation and quality control.[41,42] We found that CB5083 similarly enhanced heat shock-induced SG assembly while inhibiting the disassembly process (Figures 1H and 1I). Moreover, p97 associated with G3BP1-labeled SGs upon heat shock (Figure 1J). Significantly, neither inhibition of the components of the UPS machinery nor p97 could induce SG formation (Figure S1H), suggesting that disruption UPS per se is insufficient to trigger SG formation. Collectively, these systematic analyses concluded that the UPS inhibits the assembly of heat shock-induced SGs while promoting disassembly.

We next wondered whether the effect of the UPS on SG homeostasis is a heat shock-specific event. The immunoblotting analysis showcased that ubiquitin conjugates, including both K48- and K63-conjugated polyubiquitin chains also significantly accumulated upon arsenite treatment and declined rapidly upon arsenite withdrew (Figure S1I). Similar results were acquired during H_2O_2 treatment (Figure S1J), suggesting that ubiquitination is accelerated in response to various stress conditions. Moreover, pharmacological inhibition of ubiquitination, the proteasome or p97 using their corresponding inhibitors uniformly promoted the assembly of arsenite-induced SGs while delaying disassembly (Figures S1K–S1N). These results provided more systematic evidences to support the key role of the UPS in the homeostasis of arsenite-induced SGs. Taken together, our data demonstrated that the UPS is critical to SG homeostasis under various stress conditions.

The HRD1 ubiquitin ligase collaborates with p97 to regulate SG homeostasis in a stressor-dependent manner

The specificity of the UPS is mainly determined by ubiquitin ligases. The human genome encodes over 600 ubiquitin ligases.[41] To explore potential roles of ubiquitin ligases in SG homeostasis beyond APC/C^{Cdh1}, RNF4, and TRIM21, which have been implicated in SG homeostasis,[31–33] we employed a loss-of-function approach to examine ubiquitin ligases' roles in SG homeostasis. Since p97 specifically interacts with a panel of ubiquitin ligases,[42] we decided to narrow down to those p97-interactive ubiquitin ligases in the beginning. Among those ubiquitin ligases, the cullin-RING ubiquitin ligases (CRLs) represent significant portion[43] and activated by neddylation of cullins.[44] Therefore, we interrogated the neddylation system at first in order to investigate potential roles of CRLs in SG homeostasis in general. Consistent to previous studies,[45] we found that the neddylation was dispensable for the homeostasis of heat shock-induced SGs, since inhibiting the neddylation E1 enzyme using MLN4924 did not interfere with either heat shock-induced SG assembly or disassembly (Figures S2A–S2D). Therefore, we excluded the CRL ubiquitin ligases and focused on the rest 29 ubiquitin ligases interacting with either p97 or G3BP1 or both (Figure S2E). We then carried out an siRNA screening to identify ubiquitin ligases which could regulate the dynamics of heat shock-induced SGs (Figures S2E and S2F). Interestingly, among 29 ubiquitin ligases tested (Figure S2F; Table S1), we found that HRD1 is the only one which significantly delayed the disassembly of heat shock-induced SGs when silenced (Figures S3A and S3B). Furthermore, we observed that depletion of HRD1 also promoted the assembly of heat shock-induced SGs (Figure 2A). To exclude any potential off-target issues, we expressed an siRNA-resistant HRD1 cDNA in the U2OS-EGFP-G3BP1 reporter cell line, and found the HRD1 cDNA successfully reversed the HRD1 silencing phenotype (Figures 2B and S3C), further validating the authenticity of the siRNA phenotype. In line with those siRNA knockdown results, LS-102, a small molecule inhibitor of HRD1 dramatically stimulated heat shock-induced SG assembly while inhibiting SG disassembly (Figures 2C and 2D), further emphasizing that HRD1 regulates the homeostasis of heat shock-associated SGs. We repeated these experiments in HeLa cells and observed a similar phenotype, indicating the phenotype is not restricted to a single cell line (Figues S3D and S3E).

HRD1 is a RING finger ubiquitin ligase primarily localized to the ER membrane[37,46] (Figure 2E). Thus, we deleted the N-terminal transmembrane domain from HRD1, expressed the truncated HRD1 (ΔN) in the U2OS-EGFP-G3BP1 reporter cell line and performed siRNA rescue experiments. Compared to the wild-type HRD1 (Figures 2E–2G and S3F), the HRD1 ΔN mutant failed to restore the impaired SG disassembly in HRD1-silenced cells (Figures 2E–2G and S3F), implying the cellular localization of HRD1 is critical for its function. We also constructed a ubiquitin ligase inactivation mutant by modifying its cysteine-329 to alanine (C329A)[47] and employed the C329A mutant in the siRNA rescue experiment. Again, like the ΔN mutant, the C329A mutant was unable to reverse the siRNA phenotype (Figures 2E–2G and S3F), suggesting the ligase activity is also crucial for HRD1's role in the dynamics of heat shock-stimulated SGs. These data further showcased that HRD1 regulates SG dynamics depending on its role as an ER membrane-bound ubiquitin ligase, suggesting the ER might play some roles in the formation of heat shock-induced SGs.

Since HRD1 interacts with p97,[40,48,49] next we wondered whether their interaction could be altered during the heat shock response. As shown in Figure 2H, the interaction between HRD1 and p97 was enhanced upon heat shock treatment but reduced to the basal level when the temperature was dropped back to normal 37°C (Figure 2H). Interestingly, unlike p97 which partially colocalized with SGs (Figure 1J), HRD1 did not co-localize with G3BP1-labeled SGs upon heat shock treatment (Figure S3G), but it could promote the association of p97 and SGs (Figures 2I and 2J), as demonstrated by decreased colocalization between p97 and the heat shock-induced SGs when LS-102 was applied (Figures 2I and 2J). These data hinted that HRD1 might regulate p97's association with SGs through an indirect mechanism.

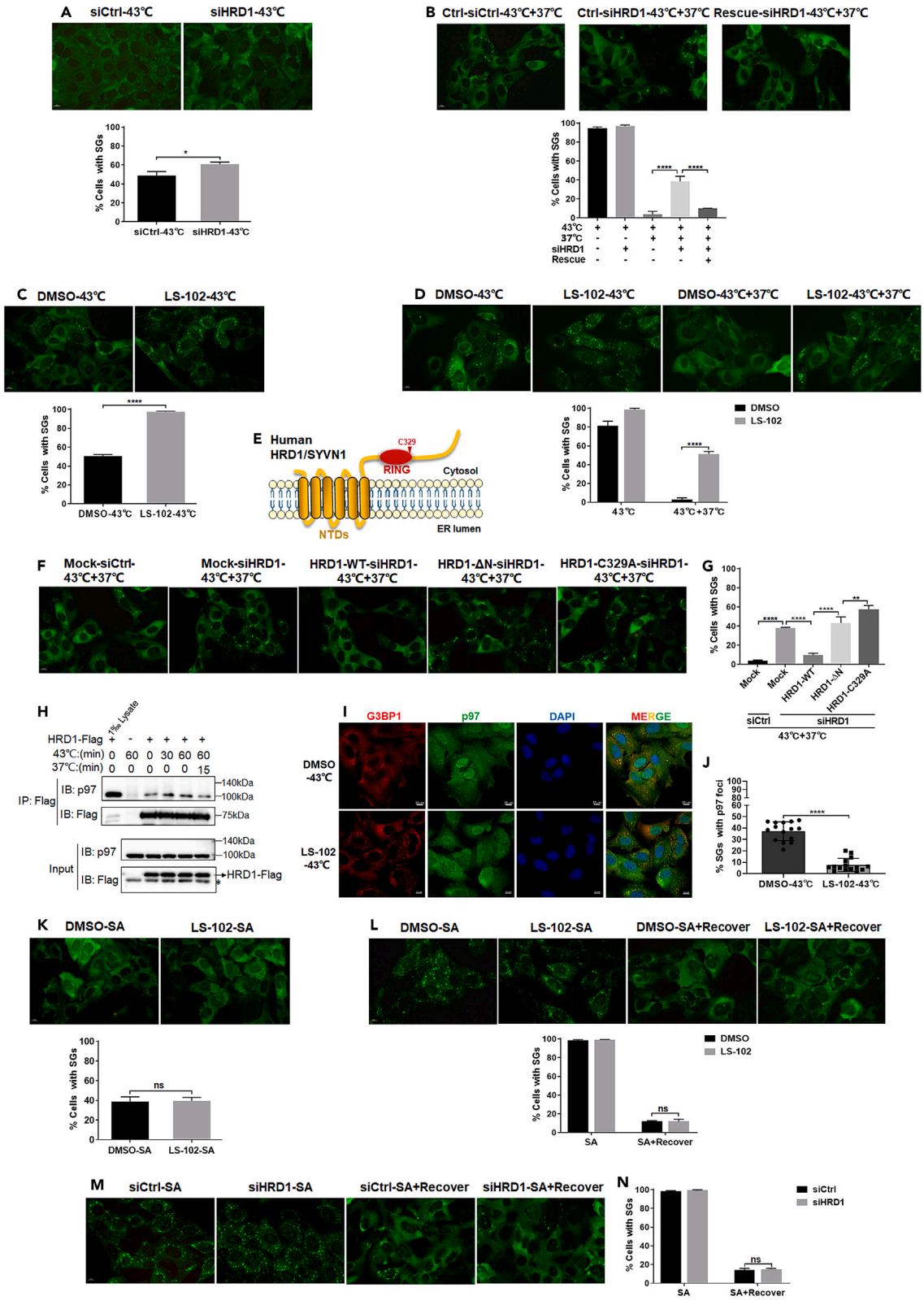
A siCtrl-43℃ siHRD1-43℃
% Cells with SGs
siCtrl-43℃ siHRD1-43℃
B Ctrl-siCtrl-43℃+37℃ Ctrl-siHRD1-43℃+37℃ Rescue-siHRD1-43℃+37℃
43℃
37℃
siHRD1
Rescue
C DMSO-43℃ LS-102-43℃
DMSO-43℃ LS-102-43℃
D DMSO-43℃ LS-102-43℃ DMSO-43℃+37℃ LS-102-43℃+37℃
DMSO
LS-102
43℃ 43℃+37℃
E Human HRD1/SYVN1
C329
RING
Cytosol
ER lumen
NTDs
F Mock-siCtrl-43℃+37℃ Mock-siHRD1-43℃+37℃ HRD1-WT-siHRD1-43℃+37℃ HRD1-ΔN-siHRD1-43℃+37℃ HRD1-C329A-siHRD1-43℃+37℃
G
Mock Mock HRD1-WT HRD1-ΔN HRD1-C329A
siCtrl siHRD1
43℃+37℃
H
1% Lysate
HRD1-Flag
43℃:(min)
37℃:(min)
IP: Flag
IB: p97
IB: Flag
Input
140kDa
100kDa
75kDa
HRD1-Flag
I G3BP1 p97 DAPI MERGE
DMSO -43℃
LS-102 -43℃
J % SGs with p97 foci
DMSO-43℃ LS-102-43℃
K DMSO-SA LS-102-SA
ns
DMSO-SA LS-102-SA
L DMSO-SA LS-102-SA DMSO-SA+Recover LS-102-SA+Recover
DMSO
LS-102
SA SA+Recover
M siCtrl-SA siHRD1-SA siCtrl-SA+Recover siHRD1-SA+Recover
N
siCtrl
siHRD1
SA SA+Recover

Figure 2. The HRD1 ubiquitin ligase collaborates with p97 to regulate SG homeostasis in a stressor-dependent manner

In (A–D) and (K and L), upper and lower panels are representative images which were taken using microscope and their corresponding quantifications and statistical analysis, respectively. $n = 3$ replicates with >450 cells per condition.

(A) The U2OS-EGFP-G3BP1 cells were transfected with siHRD1 oligos for 48 h, and then cultured at 43°C for 10 min. Data are shown as mean ± SD, unpaired two-tailed Student's t tests; $*p \leq 0.05$. Scale bar: 10 μm.

(B) The U2OS-EGFP-G3BP1 cells stably expressing HRD1 siRNA-resistant cDNA were transfected with siHRD1 oligos for 48 h, and then cultured at 43°C for 30 min followed by 37°C for 8 min. Data are shown as mean ± SD, one-way ANOVA with Tukey's multiple comparisons test; $****p \leq 0.0001$. Scale bar: 10 μm.

(C and D) The U2OS-EGFP-G3BP1 cells were pretreated using HRD1 inhibitor LS-102 for 15 min, and then cultured at 43°C for 10 min (C). Alternatively, cells were pretreated with LS-102 for 15 min and then maintained at 43°C for 30 min, or cells were cultured at 43°C with LS-102 for 30 min followed by 37°C for 8 min (D). Data are shown as mean ± SD. Unpaired two-tailed Student's t tests (C); two-way ANOVA with Sidak's multiple comparisons test (D); $****p \leq 0.0001$. Scale bar: 10 μm.

(E) Schematic illustration of human HRD1. NTD: N-Terminal transmembrane domains; RING: RING finger motif; C329: Cysteine 329 within the RING finger motif.

(F) The U2OS-EGFP-G3BP1 cells stably expressing HRD1-WT, NTD deletion, or the C329A mutant rescue cDNAs were transfected with siHRD1 oligos for 48 h, and then cultured at 43°C for 30 min followed by 37°C for 8 min. Scale bar: 10 μm.

(G) Quantifications and statistical analysis of data in (F). Data are shown as mean ± SD, one-way ANOVA with Tukey's multiple comparisons test; $**p \leq 0.01$; $****p \leq 0.0001$, $n = 3$ replicates with >450 cells per condition.

(H) The U2OS-EGFP-G3BP1 cells stably expressing HRD1-Flag-Strep were cultured at 43°C for two different time periods, or maintained at 43°C for 60 min followed by 37°C for 15 min. Cells were collected and subjected to immunoprecipitation using anti-Flag antibody, and immunoblotting using either p97 or Flag antibodies. Asterisk indicates non-specific band.

(I) U2OS cells were pretreated with LS-102 for 15 min and maintained at 43°C for 30 min. Endogenous G3BP1 and p97 localizations were shown using IF with corresponding antibodies. Scale bar: 10 μm.

(J) Quantification and statistics of p97-positive SG in (I). Data are shown as mean ± SD, unpaired two-tailed Student's t tests; $****p \leq 0.0001$, $n = 15$ with ≥1,800 SGs per condition.

(K and L) The U2OS-EGFP-G3BP1 cells were pretreated using LS-102 for 15 min, and then treated using 0.5 mM arsenite for 13 min (K). Alternatively, cells were treated with 0.5 mM arsenite along with LS-102 for 30 min, or cells were treated with 0.5 mM arsenite for 30 min and recovered in arsenite-free medium with LS-102 for 100 min (L). Data are shown as mean ± SD. Unpaired two-tailed Student's t tests (K); two-way ANOVA with Sidak's multiple comparisons test (L); ns, not significant. Scale bar: 10 μm.

(M) The U2OS-EGFP-G3BP1 cells were transfected with siHRD1 for 48 h, and treated using 0.5 mM arsenite for 30 min, or followed by recovery in arsenite-free medium for 100 min. Scale bar: 10 μm.

(N) Quantifications and statistical analysis of data in (M). Data are shown as mean ± SD, two-way ANOVA with Sidak's multiple comparisons test; ns, not significant, $n = 3$ replicates with >450 cells per condition. See also Figures S2 and S3.

Since p97 also regulates arsenite-induced SG dynamics,[35,50] we decided to determine whether HRD1 plays a similar role during the arsenite response. Surprisingly, neither pharmacological inhibition nor genetic ablation of HRD1 affected arsenite-induced SG assembly or disassembly (Figures 2K–2N). Collectively, these results demonstrated the specificity of HRD1 in regulating the homeostasis of heat shock-induced SGs, whereas p97 might play more general roles.

SEL1L cooperates with HRD1 to regulate the heat shock-induced SG homeostasis

HRD1 forms a ubiquitin ligase complex with SEL1L which stabilizes HRD1 proteins and facilitates substrate recognition by the complex[38,51] (Figure S4A). Consistently, silencing SEL1L using siRNA oligos increased the amount of the heat shock-induced SGs while inhibiting disassembly (Figures 3A, 3B, and S4B). Again, the siRNA phenotype of SEL1L in SG disassembly was fully rescued when an siRNA-resistant SEL1L cDNA was expressed in the U2OS-EGFP-G3BP1 reporter cell line (Figures 3C and S4C), demonstrating the authenticity of the siRNA phenotype. The effect of the HRD1-SEL1L complex on heat shock-induced SG disassembly was confirmed in U2OS cells by immunostaining endogenous G3BP1 (Figure S4D). Furthermore, we also constructed the EGFP-G3BP1 reporter system in HeLa cells (HeLa-EGFP-G3BP1). A comparable phenotype was detected when HRD1 or SEL1L was silenced using siRNA oligos in the HeLa-EGFP-G3BP1 reporter cell line (Figure S4E), indicating the observed phenotype is not limited to one cell line. Consistent with HRD1's specific role in the homeostasis of heat shock-induced SGs, knocking down SEL1L did not affect the dynamics of arsenite-induced SGs (Figures S4F and S4G). Together, these results uniformly demonstrated that the HRD1-SEL1L complex inhibits the assembly of SGs while promoting their disassembly in a stressor-specific manner.

Because both HRD1 and SEL1L influence the homeostasis of heat shock-induced SGs similarly, we proceeded to investigate potential alterations in the complex formation during the heat shock response. We performed a reciprocal co-immunoprecipitation (coIP) experiment and found that the interaction between HRD1 and SEL1L became stronger upon heat shock stimulation but returned to the basal level during the recovery phase (Figures 3D and 3E), indicating a coordinated action between HRD1 and SEL1L in regulating SG homeostasis. To further dissect the mechanism behind, we examined the interactions between SEL1L and various mutants of HRD1 during the heat shock response (Figure 3F). Clearly, the HRD1 ΔN truncation mutant failed to interact with SEL1L (Figure 3F), highlighting the requirement of the ER membrane retention for the HRD1-SEL1L association. Interestingly, the HRD1 C329A mutant, which lost its ubiquitin ligase activity, showed stronger interaction with SEL1L compared to the wildtype (Figure 3F). This could potentially explain the dominant negative effect of the HRD1 C329A mutant on SG homeostasis when overexpressed in U2OS-EGFP-G3BP1 reporter cells, because the mutant could compete with endogenous HRD1 for binding to endogenous SEL1L, but could not release it.

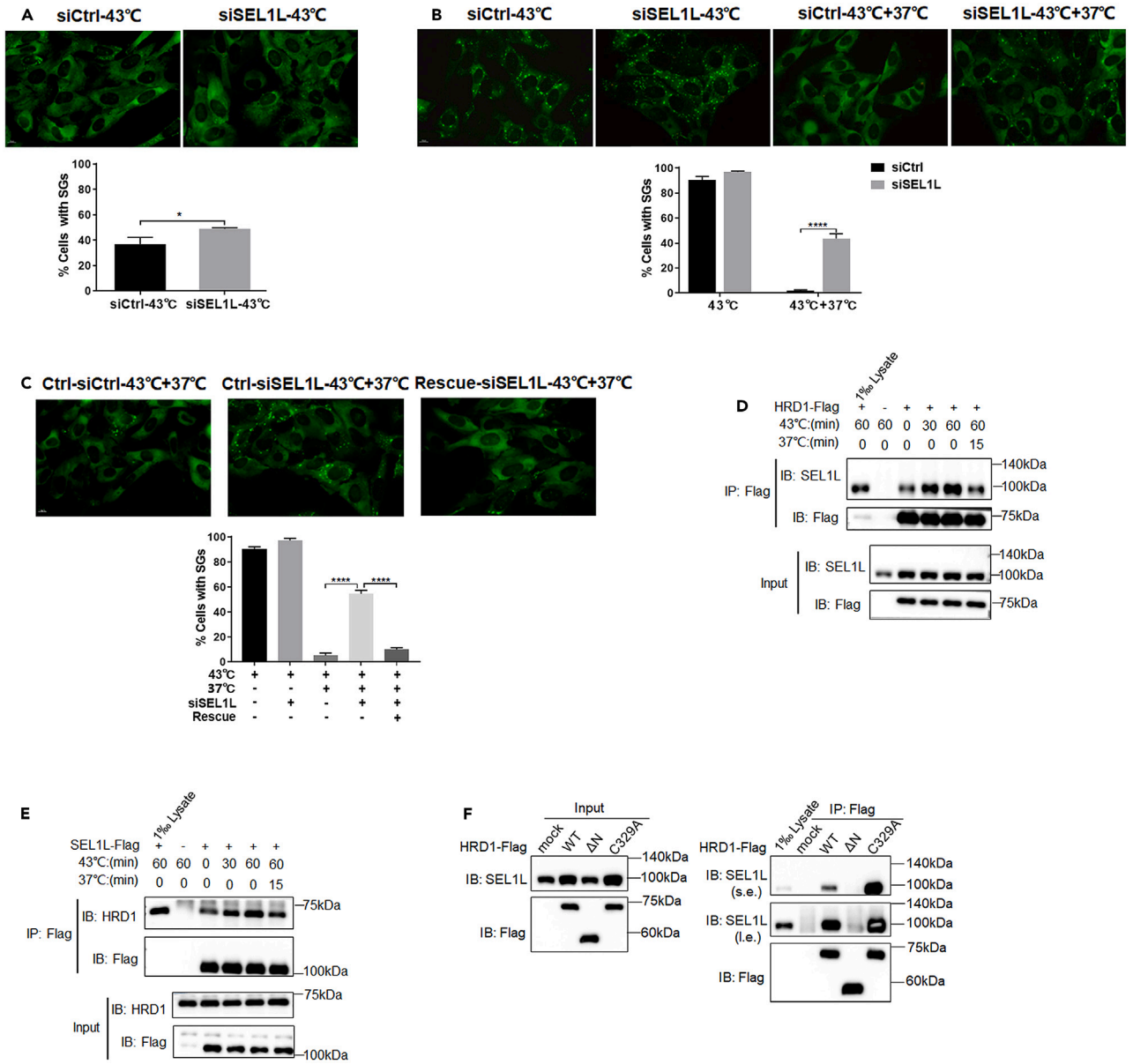

Figure 3. SEL1L cooperates with HRD1 to regulate the heat shock-induced SG homeostasis

In (A–C), upper and lower panels are representative images which were taken using microscope and their corresponding quantifications and statistical analysis, respectively. $n = 3$ replicates with >450 cells per condition.

(A and B) The U2OS-EGFP-G3BP1 cells were transfected with siSEL1L oligos for 48 h, and then maintained at 43°C for 10 min (A). Alternatively, cells were cultured at 43°C for 30 min, or followed by 37°C for 8 min (B). Data are shown as mean ± SD. Unpaired two-tailed Student's t tests (A); two-way ANOVA with Sidak's multiple comparisons test (B); *$p \leq 0.05$; ****$p \leq 0.0001$. Scale bar: 10 μm.

(C) The U2OS-EGFP-G3BP1 cells stably expressing the SEL1L siRNA-resistant cDNA were transfected with siSEL1L oligos for 48 h, then incubated at 43°C for 30 min and followed by 37°C for 8 min. Data are shown as mean ± SD, one-way ANOVA with Tukey's multiple comparisons test; ****$p \leq 0.0001$. Scale bar: 10 μm.

(D) The U2OS-EGFP-G3BP1 cells stably expressing HRD1-Flag-Strep were maintained at 43°C for different times, or incubated at 43°C for 60 min and followed by 37°C for 15 min. Cells were then collected, subjected to immunoprecipitation using anti-Flag antibody and detected using antibodies of SEL1L and Flag, respectively.

(E) Same as (D), except that the U2OS-EGFP-G3BP1 cells stably expressing SEL1L-Flag-Strep were employed for coIP using anti-Flag antibody and detected using antibodies of HRD1 and Flag, respectively.

(F) The U2OS-EGFP-G3BP1 cells stably expressing the wildtype, NTD deletion, or the C329A mutant of HRD1-Flag-Strep were collected for coIP using anti-Flag antibody and immunoblotted using antibodies of SEL1L and Flag, respectively.See also Figure S4.

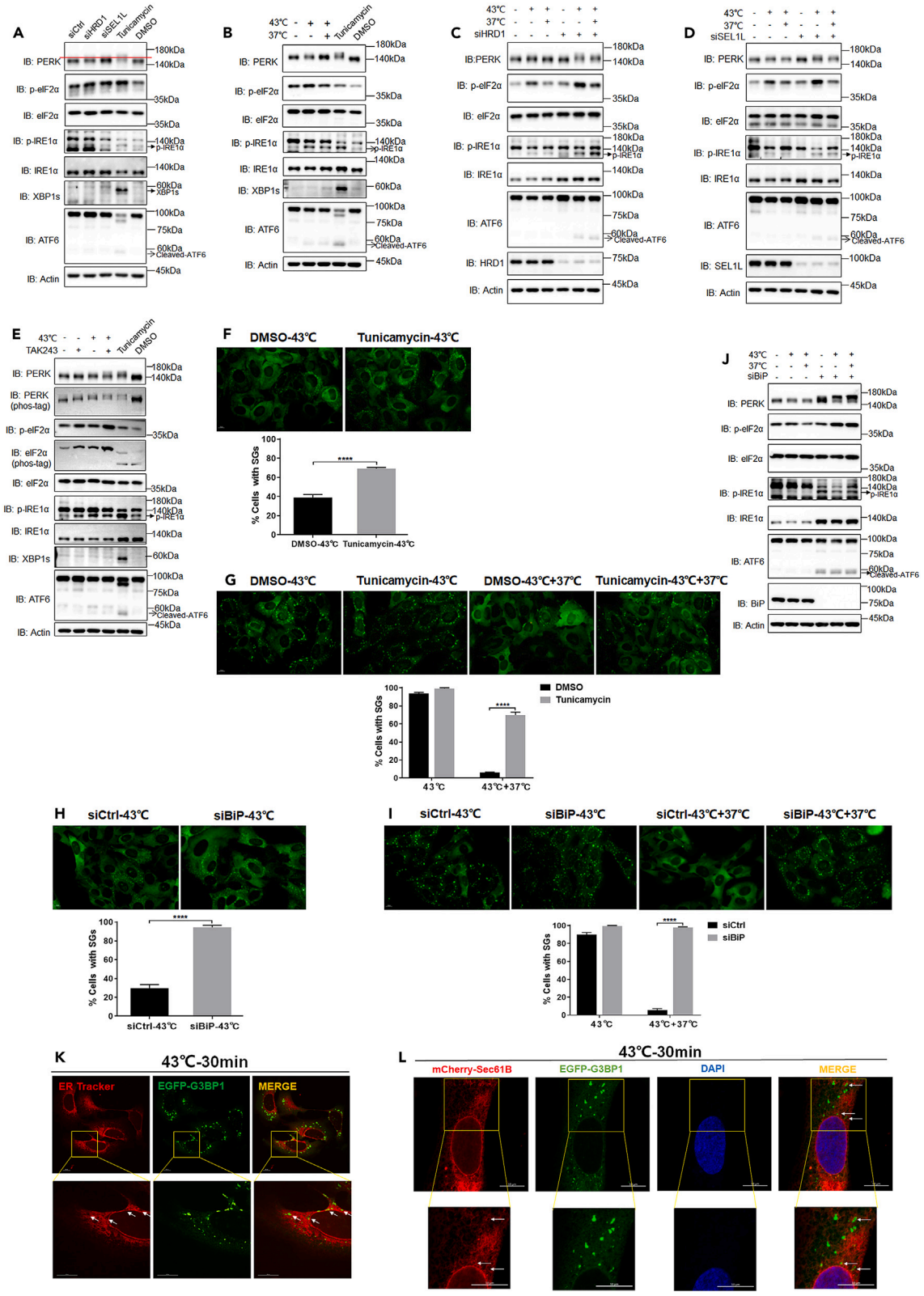
A
siCtrl
siHRD1
siSEL1L
Tunicamycin
DMSO
IB: PERK
IB: p-eIF2α
IB: eIF2α
IB: p-IRE1α
IB: IRE1α
IB: XBP1s
IB: ATF6
IB: Actin
180kDa
140kDa
35kDa
60kDa
XBP1s
100kDa
75kDa
Cleaved-ATF6
45kDa
B
43℃
37℃
C
siHRD1
IB: HRD1
D
siSEL1L
IB: SEL1L
E
TAK243
IB: PERK (phos-tag)
IB: eIF2α (phos-tag)
F
DMSO-43℃
Tunicamycin-43℃
% Cells with SGs
****
G
DMSO-43℃+37℃
Tunicamycin-43℃+37℃
DMSO
Tunicamycin
43℃
43℃+37℃
J
siBiP
IB: BiP
H
siCtrl-43℃
siBiP-43℃
I
siCtrl-43℃+37℃
siBiP-43℃+37℃
siCtrl
siBiP
K
43℃-30min
ER Tracker
EGFP-G3BP1
MERGE
L
mCherry-Sec61B
DAPI

Figure 4. ER stress promotes the heat shock-induced SG assembly while inhibiting disassembly

In (F–I), upper and lower panels are representative images which were taken using microscope and their corresponding quantifications and statistical analysis, respectively. $n = 3$ replicates with >450 cells per condition.

(A) U2OS cells were transfected with siHRD1 or siSEL1L oligos for 48 h and collected for immunoblotting using antibodies of the ER stress-related marker proteins. Tunicamycin-treated samples were employed as positive controls.

(B) U2OS cells were incubated at 43°C for 30 min, or followed by 37°C for 8 min. Cells were then collected for immunoblotting using antibodies of the ER stress-related marker proteins. Tunicamycin-treated samples were employed as positive controls.

(C and D) U2OS cells were transfected with siHRD1 (C) or siSEL1L (D) oligos for 48 h, and then maintained at 43°C for 30 min, or followed by 37°C for 8 min. Cells were collected for immunoblotting using antibodies of the ER stress-related marker proteins.

(E) U2OS cells were pretreated with TAK243 for 15 min, and then incubated at 43°C for 30 min. Cells were then collected for immunoblotting using antibodies of the ER stress-related marker proteins. Tunicamycin-treated samples were employed as positive controls. Phosphorylation of PERK or eIF2α was confirmed using phos-tag gels.

(F and G) The U2OS-EGFP-G3BP1 cells were pretreated with tunicamycin for 15 min, and then cultured at 43°C for 10 min (F). Alternatively, cells were pretreated with tunicamycin for 15 min and then incubated at 43°C for 30 min, or cells were maintained at 43°C with tunicamycin for 30 min followed by 37°C for 8 min (G). Data are shown as mean ± SD. Unpaired two-tailed Student's t tests (F); two-way ANOVA with Sidak's multiple comparisons test (G); ****$p \leq 0.0001$. Scale bar: 10 μm.

(H and I) The U2OS-EGFP-G3BP1 cells were transfected with siBiP oligos for 48 h, and then incubated at 43°C for 10 min (H). Alternatively, cells were cultured at 43°C for 30 min, or followed by 37°C for 8 min (I). Data are shown as mean ± SD. Unpaired two-tailed Student's t tests (H); two-way ANOVA with Sidak's multiple comparisons test (I); ****$p \leq 0.0001$. Scale bar: 10 μm.

(J) Same as (C) except that cells were transfected with siBiP oligos.

(K) The U2OS-EGFP-G3BP1 cells were labeled with the ER tracker and incubated at 43°C for 30 min. White arrows indicate the representative ER tubules. Scale bar: 10 μm.

(L) The U2OS-EGFP-G3BP1 cells were transfected with mCherry-Sec61B for 24 h, and maintained at 43°C for 30 min. White arrows indicate the representative ER tubules. Scale bar: 10 μm. See also Figure S5.

ER stress promotes the heat shock-induced SG assembly while inhibiting disassembly

Previous reports have shown the significance of ubiquitination in the disassembly of SGs, with G3BP1 being an essential modified target.[34] However, the specific ubiquitin ligase responsible for G3BP1 ubiquitination during heat shock remained unidentified, although TRIM21 has been demonstrated to ubiquitylate G3BP1 during arsenite-induced SG formation.[33] Initially, we thought that the HRD1-SEL1L complex could ubiquitylate G3BP1 during the heat shock response. To prove our hypothesis, we pulled out ubiquitylated proteins from heat shock-treated cells using the ThUBDs method,[52,53] and then detected ubiquitylated G3BP1 using an anti-G3BP1 antibody. We found that silencing HRD1 had negligible impact on G3BP1 ubiquitination upon heat shock stimulation (Figure S5A), implying that the HRD1-SEL1L complex is not the ubiquitin ligase of G3BP1. We also determined whether HRD1 is responsible for the alteration of TDP43 ubiquitination during the heat shock response,[31,53] but could not find any convincing evidence (Figure S5B). Moreover, we isolated the mRNPs via Oligo-dT beads, which recognize and specifically bind to the poly(A) tail of mRNAs, and then performed immunoblotting to analyze ubiquitination of mRNA-binding proteins. As previously reported,[53] the level of global ubiquitination associated with captured mRNPs was increased upon heat shock, while the inhibition of HRD1 had no obvious impact on such increment (Figure S5C), further suggesting that the HRD1-SEL1L ubiquitin ligase might regulate the homeostasis of heat-shock induced SGs via a unique mechanism.

The best-characterized function of the HRD1-SEL1L ubiquitin ligase is to facilitate the UPS-dependent degradation of mis/unfolded proteins excessively accumulated in the ER, thereby alleviating ER stress.[39,54] Therefore, we wondered whether ER stress plays any roles in the homeostasis of heat shock-induced SGs. We first knocked down the HRD1-SEL1L complex and surveyed several main events of ER stress. Indeed, silencing either HRD1 or SEL1L promoted the phosphorylation of PERK, as evidenced by its mobility shift on SDS-PAGE gels resulting from autophosphorylation[55] (Figure 4A). More profound increase was observed in the phosphorylation of its substrate, eIF2α (Figure 4A). Phosphorylation of IRE1α was also increased (Figure 4A), suggesting an enhanced ER stress response, although the cleavage of ATF6 protein, an ATF6 activation event during ER stress, was not obvious (Figure 4A). After confirming the regulatory roles of HRD1-SEL1L in ER-stress, we further examined whether ER stress is induced during heat shock and subsequently functions in the dynamics of heat shock-stimulated SGs. To test our hypothesis, we surveyed the main events of ER stress during the heat shock response. Indeed, the phosphorylation of both PERK and eIF2α was enhanced upon heat shock treatment and was reduced to the basal level during the recovery phase (Figure 4B). Interestingly, although IRE1α phosphorylation was rapidly induced upon heat shock (Figure 4B), it was maintained even when the temperature was reduced to 37°C (Figure 4B). We also observed a marginal cleavage of ATF6 upon heat shock treatment (Figure 4B). These data indicated that heat shock could activate ER stress, suggesting a potential correlation between ER stress and SG homeostasis during the heat shock response.

Next, we examined whether the heat shock-induced ER stress could be elevated when the HRD1-SEL1L ubiquitin ligase is inactivated. Indeed, silencing either HRD1 or SEL1L enhanced heat shock-induced phosphorylation of PERK, eIF2α, and IRE1α when cells were shocked at 43°C (Figures 4C and 4D). These phosphorylation events were still maintained when the temperature was reduced to 37°C (Figures 4C and 4D). Moreover, depleting either HRD1 or SEL1L promoted ATF6 cleavage under heat shock treatment (Figures 4C and 4D). We further confirmed these observations using LS-102 (Figure S5D), although LS-102 showed little impact on IRE1α phosphorylation or ATF6 cleavage in response to heat shock (Figure S5D). Notably, inactivation of the HRD1-SEL1L ubiquitin ligase per se did not induce SG formation (Figure S5E), indicating that inactivating the HRD1-SEL1L ubiquitin ligase alone is insufficient to trigger SG nucleation, but rather accelerate the heat shock-induced SG formation.

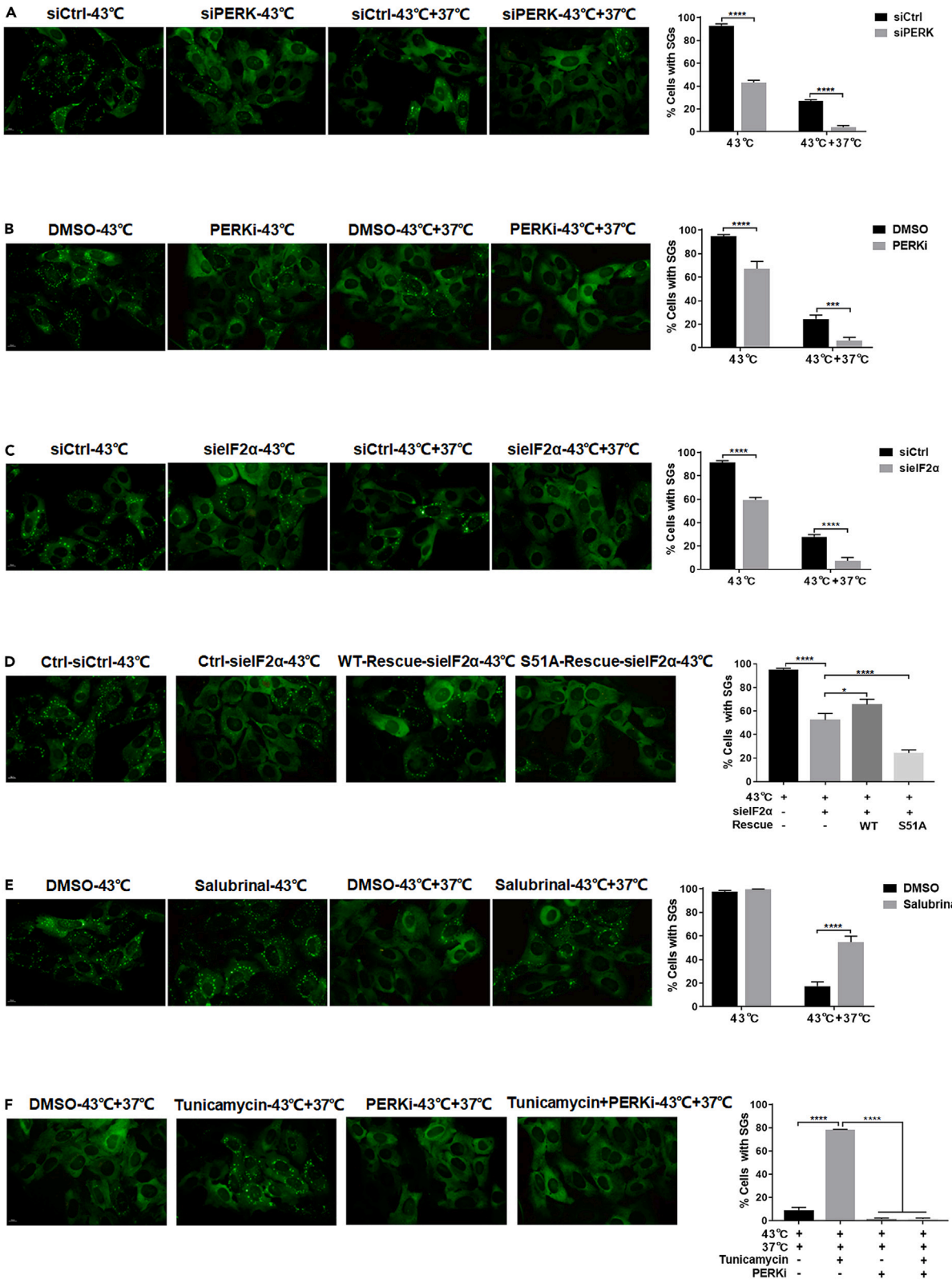
A
siCtrl-43℃
siPERK-43℃
siCtrl-43℃+37℃
siPERK-43℃+37℃
% Cells with SGs
siCtrl
siPERK
43℃
43℃+37℃
B
DMSO-43℃
PERKi-43℃
DMSO-43℃+37℃
PERKi-43℃+37℃
DMSO
PERKi
C
siCtrl-43℃
sieIF2α-43℃
siCtrl-43℃+37℃
sieIF2α-43℃+37℃
sieIF2α
D
Ctrl-siCtrl-43℃
Ctrl-sieIF2α-43℃
WT-Rescue-sieIF2α-43℃
S51A-Rescue-sieIF2α-43℃
Rescue
WT
S51A
E
DMSO-43℃
Salubrinal-43℃
DMSO-43℃+37℃
Salubrinal-43℃+37℃
Salubrinal
F
DMSO-43℃+37℃
Tunicamycin-43℃+37℃
PERKi-43℃+37℃
Tunicamycin+PERKi-43℃+37℃
37℃
Tunicamycin
PERKi

Figure 5. ER stress couples with the PERK-eIF2α axis to promote the heat shock-induced SG genesis

In all figures, left and right panels are representative images which were taken using microscope and their corresponding quantifications and statistical analysis, respectively. $n = 3$ replicates with >450 cells per condition.

(A) The U2OS-EGFP-G3BP1 cells were transfected with siPERK oligos for 48 h, and then incubated at 43°C for 30 min, or followed by 37°C for 5 min. Data are shown as mean ± SD, two-way ANOVA with Sidak's multiple comparisons test; ****$p \leq 0.0001$. Scale bar: 10 μm.

(B) The U2OS-EGFP-G3BP1 cells were pretreated with PERK inhibitor for 15 min and then incubated at 43°C for 30 min, or cells were cultured at 43°C with PERKi for 30 min followed by incubation at 37°C for 5 min. Data are shown as mean ± SD, two-way ANOVA with Sidak's multiple comparisons test; ***$p \leq 0.001$; ****$p \leq 0.0001$. Scale bar: 10 μm.

(C) Same as in (A) except that cells were transfected with sieIF2α oligos. Data are shown as mean ± SD, two-way ANOVA with Sidak's multiple comparisons test; ****$p \leq 0.0001$. Scale bar: 10 μm.

(D) The U2OS-EGFP-G3BP1 cells stably expressing either the wildtype or the S51A mutant of eIF2α rescue cDNAs were transfected with sieIF2α oligos for 48 h, and then incubated at 43°C for 30 min. Data are shown as mean ± SD, one-way ANOVA with Tukey's multiple comparisons test; *$p \leq 0.05$; ****$p \leq 0.0001$. Scale bar: 10 μm.

(E) Same as in (B) except that cells were treated with Salubrinal and recovered at 37°C for 8 min. Data are shown as mean ± SD, two-way ANOVA with Sidak's multiple comparisons test; ****$p \leq 0.0001$. Scale bar: 10 μm.

(F) The U2OS-EGFP-G3BP1 cells were incubated at 43°C with Tunicamycin, PERKi, or both for 30 min, followed by 37°C for 8 min. Data are shown as mean ± SD, one-way ANOVA with Tukey's multiple comparisons test; ****$p \leq 0.0001$. Scale bar: 10 μm. See also Figure S6.

Similarly, inactivating Uba1, the proteasome, or p97 augmented heat shock-induced phosphorylation of PERK and eIF2α, rather than IRE1α, during SG assembly (Figures 4E, S5F, and S5G), which also lasts for a time even during the recovery phase (Figures S5F and S5G). Together, these data emphasized the role of the UPS in the homeostasis of heat shock-induced SGs by regulating at least the PERK-eIF2α axis of ER stress.

To further validate the role of ER stress in regulating the dynamics of heat shock-stimulated SGs, we employed tunicamycin, a classic ER stress chemical inducer. Tunicamycin alone was incapable of inducing any SG formation (Figure S5H). However, it notably promoted the heat shock-induced SG assembly while prolonging the SG disassembly process (Figures 4F and 4G). Furthermore, using siRNA oligos to genetically deplete BiP, an ER stress repressor, we observed a significant enhancement in the heat shock-induced SG assembly and a delay in SG disassembly (Figures 4H and 4I). Consistently, silencing BiP alone resulted in an intrinsic activation of ER stress, as the phosphorylation of both PERK and IRE1α, as well as ATF6 cleavage was observed (Figure 4J), which were even sustained over the course of the heat shock-induced SG homeostasis (Figure 4J). However, like tunicamycin, knocking down BiP alone is insufficient to induce SG formation either (Figure S5I). Together, these data showed that ER stress alone could not trigger SG formation, but could promote the heat shock-induced SG assembly while delaying disassembly.

Ultimately, we captured the close vicinity of the heat shock-induced SG and the ER. Taking advantage of the ER tracker as a probe or expressing an ER marker protein Sec61B to pinpoint the ER, we found that the G3BP1-labeled SGs were wrapped up by the ER tubules (Figures 4K and 4L). Our observation is consistent with a previous study in which RNP granules were largely tethered at molecular distances to the ER in human cells.[56,57] These data further provided supporting evidence for the connection between the HRD1-mediated ER stress and the SG homeostasis in response to heat shock from a spatial perspective.

All together, these findings strongly supported that ER stress plays a significant but insufficient role in the homeostasis of heat shock-induced SGs.

ER stress couples with the PERK-eIF2α axis to promote the heat shock-induced SG genesis

To further investigate the roles of different signaling branches of ER stress in the heat shock-induced SG homeodynamics, we knocked down PERK using the siRNA method. We found that the heat shock-induced SG assembly was significantly blocked whereas the disassembly process was accelerated upon stress removal (Figures 5A and S6A). Application of GSK2606414, a selective small molecule inhibitor of PERK, produced similar results (Figure 5B). Consistently, similar phenotypes were observed when we silenced eIF2α (Figures 5C and S6B). Moreover, the SG assembly defect caused by eIF2α silencing was largely restored in the wildtype eIF2α expressing cells, but not in the phospho-defective ones (S51A) (Figures 5D and S6C). Furthermore, prolonged phosphorylation of eIF2α by a dephosphorylation inhibitor salubrinal notably delayed the heat shock-induced SG disassembly (Figure 5E), highlighting the crucial involvement of eIF2α phosphorylation at serine-51 in maintaining SG homeostasis. Collectively, these data demonstrated that the PERK-eIF2α signaling branch of ER stress is important for the homeostasis of heat shock-induced SGs.

To further investigate the contribution of the PERK-eIF2α signaling axis in the homeostasis of heat shock-induced SGs, we employed tunicamycin to block SG disassembly (Figure 5F). Abrogation of the PERK activity using GSK2606414 significantly reversed the inhibitory effect of tunicamycin on SG disassembly when heat shock was removed (Figure 5F). These results further consolidated the role of the PERK-eIF2α signaling axis in the homeostasis of heat shock-regulated SGs.

Differential effects of ER stress signaling branches on SG homeostasis under heat shock

Next, we explored potential roles of the other ER stress signaling branches in SG homeostasis beyond the PERK-eIF2α signaling axis. Indeed, depleting IRE1α using siRNA oligos also dramatically abrogated the heat shock-induced SG formation while accelerated its disassembly (Figures 6A and S6D). In line with this result, pharmacological inhibition of IRE1α using a small molecule inhibitor, named Kira6, similarly

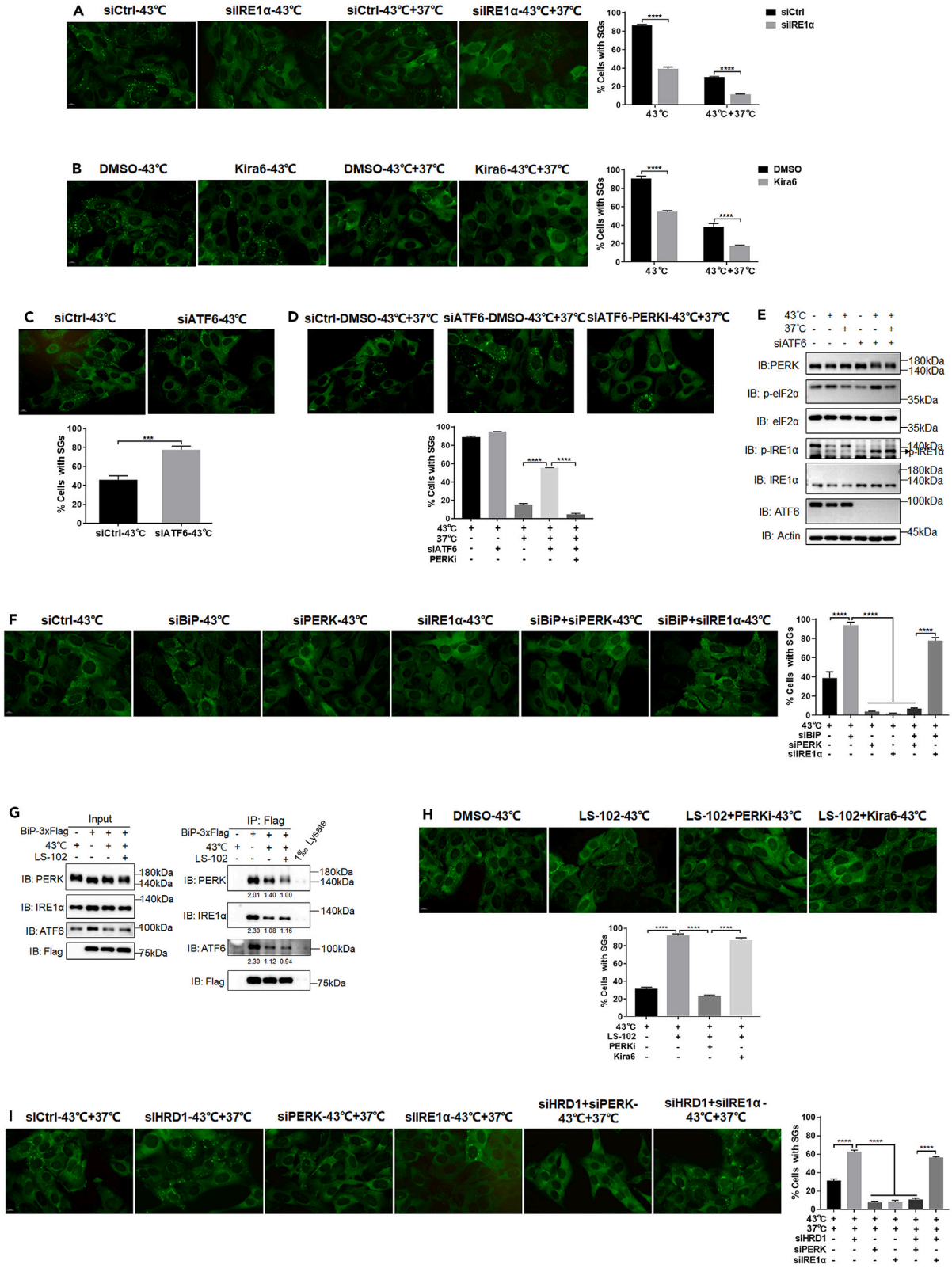
A
siCtrl-43℃
siIRE1α-43℃
siCtrl-43℃+37℃
siIRE1α-43℃+37℃
% Cells with SGs
siCtrl
siIRE1α
43℃
43℃+37℃
B
DMSO-43℃
Kira6-43℃
DMSO-43℃+37℃
Kira6-43℃+37℃
DMSO
Kira6
C
siCtrl-43℃
siATF6-43℃
D
siCtrl-DMSO-43℃+37℃
siATF6-DMSO-43℃+37℃
siATF6-PERKi-43℃+37℃
E
IB:PERK
IB: p-eIF2α
IB: eIF2α
IB: p-IRE1α
IB: IRE1α
IB: ATF6
IB: Actin
F
siCtrl-43℃
siBiP-43℃
siPERK-43℃
siIRE1α-43℃
siBiP+siPERK-43℃
siBiP+siIRE1α-43℃
G
Input
IP: Flag
BiP-3xFlag
LS-102
IB: PERK
IB: IRE1α
IB: ATF6
IB: Flag
1% Lysate
H
DMSO-43℃
LS-102-43℃
LS-102+PERKi-43℃
LS-102+Kira6-43℃
I
siCtrl-43℃+37℃
siHRD1-43℃+37℃
siPERK-43℃+37℃
siIRE1α-43℃+37℃
siHRD1+siPERK-43℃+37℃
siHRD1+siIRE1α-43℃+37℃

Figure 6. Differential effects of ER stress signaling branches on SG homeostasis under heat shock

In (A), (B), (F) and (I), left panel and right panel are representative images which were taken using microscope and their corresponding quantifications and statistical analysis, respectively. Similarly, in (C), (D) and (H), upper and lower panels are representative images and their corresponding quantifications and statistical analysis, respectively. $n = 3$ replicates with >450 cells per condition.

(A) The U2OS-EGFP-G3BP1 cells were transfected with siIRE1α oligos for 48 h, and then maintained at 43°C for 30 min, or followed by 37°C for 5 min. Data are shown as mean ± SD, two-way ANOVA with Sidak's multiple comparisons test; ****$p \leq 0.0001$. Scale bar: 10 μm.

(B) The U2OS-EGFP-G3BP1 cells were pretreated with Kira6 for 15 min and then incubated at 43°C for 30 min, or cells were maintained at 43°C with Kira6 for 30 min followed by 37°C for 5 min. Data are shown as mean ± SD, two-way ANOVA with Sidak's multiple comparisons test; ****$p \leq 0.0001$. Scale bar: 10 μm.

(C) The U2OS-EGFP-G3BP1 cells were transfected with siATF6 oligos for 48 h, and then incubated at 43°C for 10 min. Data are shown as mean ± SD, unpaired two-tailed Student's t tests; ***$p \leq 0.001$. Scale bar: 10 μm.

(D) The U2OS-EGFP-G3BP1 cells were transfected with siATF6 oligos for 48 h, and then maintained at 43°C for 30 min, or cells were cultured at 43°C with PERKi for 30 min followed by 37°C for 8 min. Data are shown as mean ± SD, one-way ANOVA with Tukey's multiple comparisons test; ****$p \leq 0.0001$. Scale bar: 10 μm.

(E) U2OS cells were transfected with siATF6 oligos for 48 h, and then incubated at 43°C for 30 min, or followed by 37°C for 8 min. Cells were then collected for immunoblotting using antibodies of the ER stress-related marker proteins.

(F) The U2OS-EGFP-G3BP1 cells were transfected with siBiP, siPERK, or siIRE1α oligos separately or simultaneously for 48 h, and then maintained at 43°C for 10 min. Data are shown as mean ± SD, one-way ANOVA with Tukey's multiple comparisons test; ****$p \leq 0.0001$. Scale bar: 10 μm.

(G) U2OS cells were transfected with 3xFlag-BiP for 24 h, pretreated using LS-102 for 15 min and then incubated at 43°C for 30 min. Cells were collected for coIP using anti-Flag antibody and immunoblotting using antibodies of PERK, IRE1α, ATF6, and Flag. The number represents relative blotting intensity of each band above.

(H) The U2OS-EGFP-G3BP1 cells were pretreated with LS-102 either separately or simultaneously with PERKi or Kira6 for 15 min, and then cultured at 43°C for 10 min. Data are shown as mean ± SD, one-way ANOVA with Tukey's multiple comparisons test; ****$p \leq 0.0001$. Scale bar: 10 μm.

(I) The U2OS-EGFP-G3BP1 cells were transfected with siHRD1, siPERK, or siIRE1α oligos separately or simultaneously for 48 h, and then incubated at 43°C for 30 min followed by 37°C for 5 min. Data are shown as mean ± SD, one-way ANOVA with Tukey's multiple comparisons test; ****$p \leq 0.0001$. Scale bar: 10 μm. See also Figure S6.

disrupted SG assembly while promoting SG disassembly (Figure 6B). These observations suggested that IRE1α also functions in the heat shock-stimulated SG homeostasis similarly as PERK does. However, in contrast to PERK or IRE1α, silencing ATF6 significantly promoted the heat shock-induced SG assembly while inhibiting the disassembly (Figures 6C and 6D). Interestingly, inhibiting PERK completely blocked the inhibitory effect on SG disassembly resulting from the depletion of ATF6 (Figure 6D). These results indicated that an underlying interplay exists between ER stress branches upon heat shock, and the ATF6 pathway could function as a negative feedbacker in the homeostasis of heat shock-stimulated SGs. Indeed, the depletion of ATF6 upregulated the PERK-eIF2α signaling axis as well as IRE1α phosphorylation in response to heat shock (Figure 6E).

Although depleting either PERK or IRE1α impaired the heat shock-induced SG assembly, knocking down PERK rather than IRE1α completely erased the augment of SG assembly in the BiP-silenced cells (Figures 6F and S6E). During the heat shock response, PERK, IRE1α, and ATF6 were released from BiP to transduce ER stress signals as expected (Figure 6G). However, it was PERK, but not IRE1α or ATF6, that showed elevated release from BiP when HRD1 was simultaneously inhibited (Figure 6G), suggesting BiP as a mediator for HRD1 to regulate PERK-eIF2α's function in the heat shock-regulated SG homeostasis, whereas both IRE1α and ATF6 employ alternative mechanisms to control the heat shock-induced SG homeostasis. Both PERK and IRE1α exhibited analogous phenotype in the context of heat shock-induced SG homeodynamics (Figures 5A, 5B, 6A, and 6B), with their phosphorylation being modulated by the HRD1-SEL1L complex (Figures 4C and 4D). However, specifically inhibiting PERK, rather than IRE1α, completely abolishes the enhancing effect on heat shock-induced SG assembly caused by HRD1 inhibition (Figure 6H). These data indicated that it is PERK but not IRE1α connecting HRD1 to the regulation of SG homeostasis. We next did similar experiments to evaluate their effects on SG disassembly. Inactivating either PERK or IRE1α accelerated SG disassembly when HRD1 levels are maintained as expected (Figure S6F). Intriguingly, inhibiting PERK rather than IRE1α completely reversed the impaired SG disassembly in the HRD1-silenced cells (Figure S6F). Consistently, knockdown of PERK, as opposed to IRE1α, fully reversed the impaired SG disassembly in HRD1-silenced cells (Figure 6I). These results collectively indicated distinct roles for PERK and IRE1α in the HRD1-regulated SG dynamics. Specifically, PERK functions at downstream of HRD1 and is required for HRD1 to regulate the heat shock-induced SG homeostasis.

Altogether, our data demonstrated that different signaling branches of ER stress influence the heat shock-regulated SG homeostasis via distinctive mechanisms. Meanwhile, the HRD1-SEL1L complex mediates SG homeostasis mainly through the BiP-coupled PERK-eIF2α signaling axis of ER stress.

DISCUSSION

SGs are membraneless organelles induced by various stress stimuli.[1,3,6] They are important for cells to deal with hostile environments. Considering the wide diversity of stress conditions, it is reasonable to believe that SG homeostasis can be regulated through distinctive mechanisms. Protein ubiquitination is often activated in response to stress conditions.[53,58] Although still controversial, possibly due to different cell types employed, variations in experimental conditions, such as different stress treatments, time points selections in different studies or even different durations of inhibitor treatments,[34,45,59,60] recent studies indicated that ubiquitination is indeed involved in SG assembly and disassembly under heat shock or arsenite treatment.[31,33,34,60] In this study, we proved that the UPS is important for SG homeostasis during heat shock or arsenite condition by systematic loss-of-function analysis of several key factors in the UPS machinery. More importantly, we identified

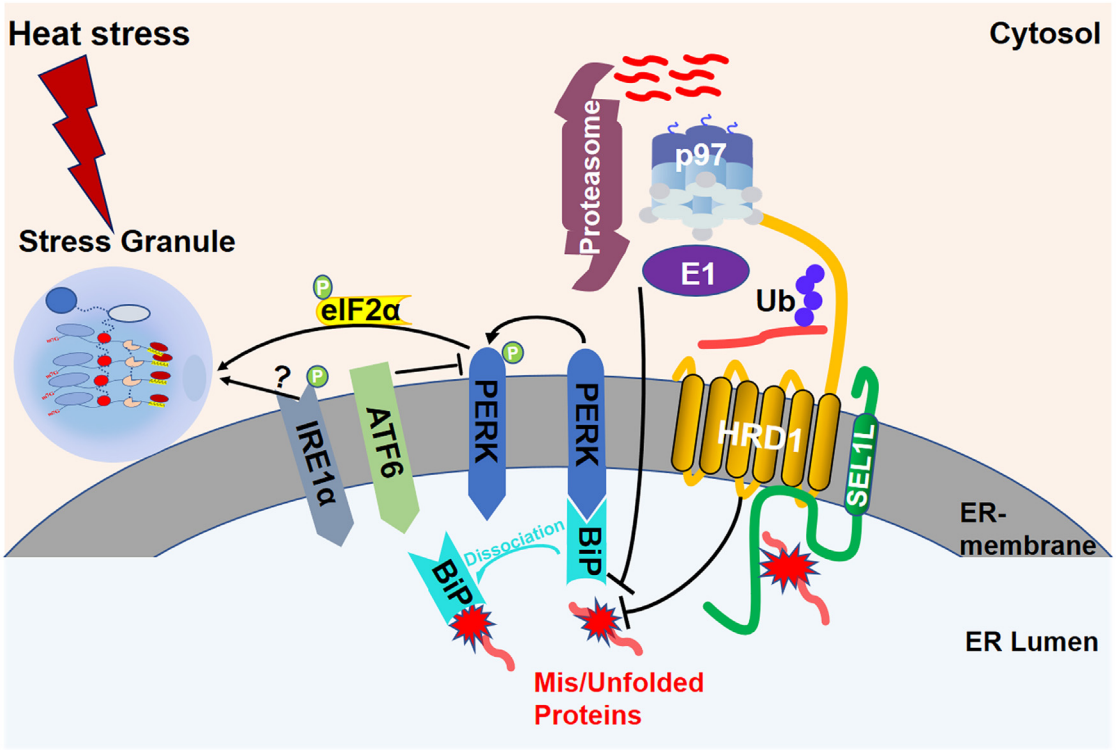

Figure 7. A proposed working model

Extracellular heat stress results in formation of SGs and concomitant overload of mis/unfolded protein in the ER. These overloaded lesions are detected by the UPR governing protein BiP, which then dissociates from the UPR transducers PERK, IRE1α, and ATF6, thereby releasing their activities. PERK then phosphorylates eIF2α at its S51 site, leading to a global translation arrest and ultimately promoting SG assembly. In response to heat shock, the HRD1-SEL1L ubiquitin ligase appears to relieve ER stress by ubiquitylating mis/unfolded proteins in the ER and then sending those ubiquitylated proteins to the proteasome in coordination with p97 for turnover. The HRD1-SEL1L ubiquitin ligase regulates the SG homeostasis via the BiP-PERK-eIF2α axis. ATF6 seems to regulate the SG formation via a negative feedback mechanism to counteract SG assembly by suppressing PERK and IRE1α signaling branches during this process, although how IRE1α showed synergistic effect with PERK remain unknown.

a RING finger ubiquitin ligase HRD1 and its associated cofactor SEL1L as regulators of the heat shock-induced SG homeostasis specifically in a ubiquitination and p97-dependent manner. Moreover, certain signaling branches of ER stress are activated under heat shock and controlled by the HRD1-SEL1L ubiquitin ligase. Finally, we demonstrated the HRD1-SEL1L ubiquitin ligase regulates the heat shock-induced SG homeostasis mainly through ER stress coupled with the PERK-eIF2α signaling axis. Based on these findings, we proposed a working model for the HRD1-SEL1L ubiquitin ligase to maintain SG homeostasis in a stressor-dependent manner (Figure 7). Heat shock results in SG formation and concomitant overload of mis/unfolded proteins in the ER. The accumulation of these excessive mis/unfolded proteins is sensed by a unfolded protein response (UPR) regulator BiP, leading to its dissociation from the UPR transducers PERK, IRE1α, and ATF6, consequently turning on their activities. PERK then phosphorylates eIF2α at its S51 site, which then leads to a global translation arrest and ultimately promotes SG assembly. The HRD1 ubiquitin ligase appears to be a negative feedbacker of SG formation, releases ER stress by ubiquitylating mis/unfolded proteins in the ER and then sending those ubiquitylated proteins to the proteasome in coordination with p97 for turnover. We observed that HRD1 forms more protein complexes with SEL1L during the heat shock treatment and less when temperature was dropped to 37°C, supporting our hypothesis. More importantly, silencing RNF185, another ER-associated ubiquitin ligase,[61,62] produced no effect on the heat shock-induced SG homeostasis (Figures S2F, S5J, and S5K), further emphasizing the specificity of the HRD1-SEL1L ubiquitin ligase in the heat shock-stimulated SG genesis.

ER stress mainly initiates three branches of signaling events.[63,64] Our results indicated that heat shock stimulates phosphorylation of PERK, eIF2α, and IRE1α, as well as the ATF6 cleavage, suggesting that all of the three signaling branches could be activated by heat shock. However, we did not observe obvious alternative splicing of XBP1, indicating the IRE1α-XBP1 signaling branch is not fully activated, possibly because we only performed a short period of heat shock treatment. While the primary function of IRE1α's kinase activity is self-phosphorylation to activate its ribonuclease activity,[65] it is still possible that the kinase activity of IRE1α might influence the dynamics of SGs through an unknown mechanism. This assumption arises from the observation that silencing IRE1α resulted in a similar phenotype to that obtained by knocking down PERK. In the case of the ATF6 signaling branch, we only observed a little bit cleavage of ATF6 during the heat shock response. Interestingly, knocking down ATF6 using siRNA oligos produced an opposite result compared to that achieved by silencing either PERK or IRE1α, implying

negative interactions among different branches of ER stress. However, it is less possible to observe any direct roles of ATF6, due to the short period of heat shock treatment in our study. Instead, ATF6 could regulate the dynamics of heat shock-induced SGs via its transcriptional targets.

Our data indicated that the HRD1-SEL1L ubiquitin ligase regulates the heat shock- but not arsenite-induced SG homeostasis, proving the specificity of this protein complex in SG dynamics. Future studies are still needed to investigate whether this ubiquitin ligase affects other stressors-induced SG assembly or disassembly and which ubiquitin ligase regulates arsenite-induced SG homeostasis in coordinating with p97. Our finding that the HRD1-SEL1L ubiquitin ligase mediates the heat shock-induced SG dynamics in couple with the BiP-PERK-eIF2α signaling axis of ER stress is consistent with the observations that inactivation of multiple UPS components, including Uba1, p97, and the proteasome could significantly enhance the phosphorylation of both PERK and eIF2α. These results well supported our main conclusion.

The aberrant SG homeostasis has been linked to human diseases, including neurodegenerative disorders and cancers.[13,15,66–68] The newly identified HRD1-SEL1L ubiquitin ligase as a regulator of the heat shock-induced SG homeostasis, could provide valuable insights into the underlying mechanisms of cellular stress responses and help make progress in future human disease treatment.

Limitations of the study

Both PERK and IRE1α exhibit analogous phenotype in SG homeostasis, with their phosphorylation being modulated by the HRD1-SEL1L ubiquitin ligase. Intriguingly, PERK, but not IRE1α, is required for HRD1 to regulate heat shock-induced SG homeostasis, while IRE1α potentially employs an alternative mechanism in the process. Further investigation is needed to reveal the underlying mechanism by which IRE1α regulates SG homeostasis under distinct stress conditions.

STAR★METHODS

Detailed methods are provided in the online version of this paper and include the following:

- KEY RESOURCES TABLE
- RESOURCE AVAILABILITY
  - Lead contact
  - Materials availability
  - Data and code availability
- EXPERIMENTAL MODEL AND STUDY PARTICIPANT DETAILS
  - Cell culture
- METHOD DETAILS
  - Establishing stable cell lines
  - Plasmid construction
  - RNA interference
  - SG assembly/disassembly and chemicals treatments
  - Western blot
  - Co-Immunoprecipitation (co-IP)
  - Immunofluorescence and microscopic imaging
- QUANTIFICATION AND STATISTICAL ANALYSIS

SUPPLEMENTAL INFORMATION

Supplemental information can be found online at https://doi.org/10.1016/j.isci.2024.110196.

ACKNOWLEDGMENTS

We thank Dr. Xin-Hua Feng and Dr. Shengda Lin for their insightful comments to this work. We also thank Dr. Wenping Li for his constructive discussion on the manuscript. This work was partially supported by grants from National Key Research and Development Program of China (No. 2022YFC3401500), the National Natural Science Foundation of China (Nos. 31970734 and 32150014), and the Fundamental Research Funds for the Central Universities. We are also grateful to our colleagues at the core facility of the Life Sciences Institute for their assistance.

AUTHOR CONTRIBUTIONS

W.S. performed the majority of the experiments, R.D. purified the ThUBDs beads and conducted the ThUBDs assay for TDP43, Y.C., F.J., J.J., and W.M. provided critical reagents. W.S. and J.J. analyzed all the data. W.S. prepared the figures. W.S. and J.J. cowrote the manuscript. W.S., J.J., and Y.C. edited the manuscript; J.J. designed and supervised the project. All authors read and approved the final manuscript.

DECLARATION OF INTERESTS

The authors declare no competing interests.

Received: November 23, 2023
Revised: March 22, 2024
Accepted: June 3, 2024
Published: June 6, 2024

REFERENCES

1. Protter, D.S.W., and Parker, R. (2016). Principles and Properties of Stress Granules. Trends Cell Biol. *26*, 668–679. https://doi.org/10.1016/j.tcb.2016.05.004.
2. Panas, M.D., Ivanov, P., and Anderson, P. (2016). Mechanistic insights into mammalian stress granule dynamics. J. Cell Biol. *215*, 313–323. https://doi.org/10.1083/jcb.201609081.
3. Anderson, P., and Kedersha, N. (2009). Stress granules. Curr. Biol. *19*, R397–R398. https://doi.org/10.1016/j.cub.2009.03.013.
4. Kedersha, N., Panas, M.D., Achorn, C.A., Lyons, S., Tisdale, S., Hickman, T., Thomas, M., Lieberman, J., McInerney, G.M., Ivanov, P., and Anderson, P. (2016). G3BP-Caprin1-USP10 complexes mediate stress granule condensation and associate with 40S subunits. J. Cell Biol. *212*, 845–860. https://doi.org/10.1083/jcb.201508028.
5. Kedersha, N.L., Gupta, M., Li, W., Miller, I., and Anderson, P. (1999). RNA-binding proteins TIA-1 and TIAR link the phosphorylation of eIF-2 alpha to the assembly of mammalian stress granules. J. Cell Biol. *147*, 1431–1442. https://doi.org/10.1083/jcb.147.7.1431.
6. Buchan, J.R., and Parker, R. (2009). Eukaryotic stress granules: the ins and outs of translation. Mol. Cell *36*, 932–941. https://doi.org/10.1016/j.molcel.2009.11.020.
7. Jain, S., Wheeler, J.R., Walters, R.W., Agrawal, A., Barsic, A., and Parker, R. (2016). ATPase-Modulated Stress Granules Contain a Diverse Proteome and Substructure. Cell *164*, 487–498. https://doi.org/10.1016/j.cell.2015.12.038.
8. Yang, P., Mathieu, C., Kolaitis, R.M., Zhang, P., Messing, J., Yurtsever, U., Yang, Z., Wu, J., Li, Y., Pan, Q., et al. (2020). G3BP1 Is a Tunable Switch that Triggers Phase Separation to Assemble Stress Granules. Cell *181*, 325–345.e28. https://doi.org/10.1016/j.cell.2020.03.046.
9. Molliex, A., Temirov, J., Lee, J., Coughlin, M., Kanagaraj, A.P., Kim, H.J., Mittag, T., and Taylor, J.P. (2015). Phase separation by low complexity domains promotes stress granule assembly and drives pathological fibrillization. Cell *163*, 123–133. https://doi.org/10.1016/j.cell.2015.09.015.
10. Bentmann, E., Haass, C., and Dormann, D. (2013). Stress granules in neurodegeneration–lessons learnt from TAR DNA binding protein of 43 kDa and fused in sarcoma. FEBS J. *280*, 4348–4370. https://doi.org/10.1111/febs.12287.
11. Mateju, D., Franzmann, T.M., Patel, A., Kopach, A., Boczek, E.E., Maharana, S., Lee, H.O., Carra, S., Hyman, A.A., and Alberti, S. (2017). An aberrant phase transition of stress granules triggered by misfolded protein and prevented by chaperone function. EMBO J. *36*, 1669–1687. https://doi.org/10.15252/embj.201695957.
12. Ganassi, M., Mateju, D., Bigi, I., Mediani, L., Poser, I., Lee, H.O., Seguin, S.J., Morelli, F.F., Vinet, J., Leo, G., et al. (2016). A Surveillance Function of the HSPB8-BAG3-HSP70 Chaperone Complex Ensures Stress Granule Integrity and Dynamism. Mol. Cell *63*, 796–810. https://doi.org/10.1016/j.molcel.2016.07.021.
13. Buchan, J.R. (2014). mRNP granules. Assembly, function, and connections with disease. RNA Biol. *11*, 1019–1030. https://doi.org/10.4161/15476286.2014.972208.
14. Taylor, J.P., Brown, R.H., Jr., and Cleveland, D.W. (2016). Decoding ALS: from genes to mechanism. Nature *539*, 197–206. https://doi.org/10.1038/nature20413.
15. Ramaswami, M., Taylor, J.P., and Parker, R. (2013). Altered ribostasis: RNA-protein granules in degenerative disorders. Cell *154*, 727–736. https://doi.org/10.1016/j.cell.2013.07.038.
16. Wang, B., Maxwell, B.A., Joo, J.H., Gwon, Y., Messing, J., Mishra, A., Shaw, T.I., Ward, A.L., Quan, H., Sakurada, S.M., et al. (2019). ULK1 and ULK2 Regulate Stress Granule Disassembly Through Phosphorylation and Activation of VCP/p97. Mol. Cell *74*, 742–757.e8. https://doi.org/10.1016/j.molcel.2019.03.027.
17. Hofmann, S., Kedersha, N., Anderson, P., and Ivanov, P. (2021). Molecular mechanisms of stress granule assembly and disassembly. Biochim. Biophys. Acta. Mol. Cell Res. *1868*, 118876. https://doi.org/10.1016/j.bbamcr.2020.118876.
18. Tsai, N.P., Ho, P.C., and Wei, L.N. (2008). Regulation of stress granule dynamics by Grb7 and FAK signalling pathway. EMBO J. *27*, 715–726. https://doi.org/10.1038/emboj.2008.19.
19. Duan, Y., Du, A., Gu, J., Duan, G., Wang, C., Gui, X., Ma, Z., Qian, B., Deng, X., Zhang, K., et al. (2019). PARylation regulates stress granule dynamics, phase separation, and neurotoxicity of disease-related RNA-binding proteins. Cell Res. *29*, 233–247. https://doi.org/10.1038/s41422-019-0141-z.
20. Huang, C., Chen, Y., Dai, H., Zhang, H., Xie, M., Zhang, H., Chen, F., Kang, X., Bai, X., and Chen, Z. (2020). UBAP2L arginine methylation by PRMT1 modulates stress granule assembly. Cell Death Differ. *27*, 227–241. https://doi.org/10.1038/s41418-019-0350-5.
21. Sidrauski, C., McGeachy, A.M., Ingolia, N.T., and Walter, P. (2015). The small molecule ISRIB reverses the effects of eIF2α phosphorylation on translation and stress granule assembly. Elife *4*, e05033. https://doi.org/10.7554/eLife.05033.
22. Pakos-Zebrucka, K., Koryga, I., Mnich, K., Ljujic, M., Samali, A., and Gorman, A.M. (2016). The integrated stress response. EMBO Rep. *17*, 1374–1395. https://doi.org/10.15252/embr.201642195.
23. Manjunath, L., Oh, S., Ortega, P., Bouin, A., Bournique, E., Sanchez, A., Martensen, P.M., Auerbach, A.A., Becker, J.T., Seldin, M., et al. (2023). APOBEC3B drives PKR-mediated translation shutdown and protects stress granules in response to viral infection. Nat. Commun. *14*, 820. https://doi.org/10.1038/s41467-023-36445-9.
24. Shi, J., Li, Z., Xu, R., Zhang, J., Zhou, Q., Gao, R., Lu, H., Lan, Y., Zhao, K., He, H., et al. (2022). The PERK/PKR-eIF2α Pathway Negatively Regulates Porcine Hemagglutinating Encephalomyelitis Virus Replication by Attenuating Global Protein Translation and Facilitating Stress Granule Formation. J. Virol. *96*, e0169521. https://doi.org/10.1128/JVI.01695-21.
25. Zhang, P., Li, Y., Xia, J., He, J., Pu, J., Xie, J., Wu, S., Feng, L., Huang, X., and Zhang, P. (2014). IPS-1 plays an essential role in dsRNA-induced stress granule formation by interacting with PKR and promoting its activation. J. Cell Sci. *127*, 2471–2482. https://doi.org/10.1242/jcs.139626.
26. McEwen, E., Kedersha, N., Song, B., Scheuner, D., Gilks, N., Han, A., Chen, J.J., Anderson, P., and Kaufman, R.J. (2005). Heme-regulated inhibitor kinase-mediated phosphorylation of eukaryotic translation initiation factor 2 inhibits translation, induces stress granule formation, and mediates survival upon arsenite exposure. J. Biol. Chem. *280*, 16925–16933. https://doi.org/10.1074/jbc.M412882200.
27. Wu, Z., Mei, F., Gan, Y., Liu, A., Hu, J., Jin, Y., and Yin, Y. (2023). FAM69C functions as a kinase for eIF2α and promotes stress granule assembly. EMBO Rep. *24*, e55641. https://doi.org/10.15252/embr.202255641.
28. Hershko, A., and Ciechanover, A. (1998). The ubiquitin system. Annu. Rev. Biochem. *67*, 425–479. https://doi.org/10.1146/annurev.biochem.67.1.425.
29. Komander, D., and Rape, M. (2012). The ubiquitin code. Annu. Rev. Biochem. *81*, 203–229. https://doi.org/10.1146/annurev-biochem-060310-170328.
30. Jin, J., and Harper, J.W. (2002). RING finger specificity in SCF-driven protein destruction. Dev. Cell *2*, 685–687. https://doi.org/10.1016/s1534-5807(02)00194-6.
31. Keiten-Schmitz, J., Wagner, K., Piller, T., Kaulich, M., Alberti, S., and Müller, S. (2020). The Nuclear SUMO-Targeted Ubiquitin Quality Control Network Regulates the Dynamics of Cytoplasmic Stress Granules. Mol. Cell *79*, 54–67.e7. https://doi.org/10.1016/j.molcel.2020.05.017.
32. Valdez-Sinon, A.N., Lai, A., Shi, L., Lancaster, C.L., Gokhale, A., Faundez, V., and Bassell, G.J. (2020). Cdh1-APC Regulates Protein Synthesis and Stress Granules in Neurons through an FMRP-Dependent Mechanism. iScience *23*, 101132. https://doi.org/10.1016/j.isci.2020.101132.
33. Yang, C., Wang, Z., Kang, Y., Yi, Q., Wang, T., Bai, Y., and Liu, Y. (2023). Stress granule homeostasis is modulated by TRIM21-mediated ubiquitination of G3BP1 and autophagy-dependent elimination of stress granules. Autophagy *19*, 1934–1951. https://doi.org/10.1080/15548627.2022.2164427.
34. Gwon, Y., Maxwell, B.A., Kolaitis, R.M., Zhang, P., Kim, H.J., and Taylor, J.P. (2021). Ubiquitination of G3BP1 mediates stress granule disassembly in a context-specific manner. Science *372*, eabf6548. https://doi.org/10.1126/science.abf6548.
35. Turakhiya, A., Meyer, S.R., Marincola, G., Böhm, S., Vanselow, J.T., Schlosser, A.,

Hofmann, K., and Buchberger, A. (2018). ZFAND1 Recruits p97 and the 26S Proteasome to Promote the Clearance of Arsenite-Induced Stress Granules. Mol. Cell *70*, 906–919.e7. https://doi.org/10.1016/j.molcel.2018.04.021.

36. Deng, L., Meng, T., Chen, L., Wei, W., and Wang, P. (2020). The role of ubiquitination in tumorigenesis and targeted drug discovery. Signal Transduct. Target. Ther. *5*, 11. https://doi.org/10.1038/s41392-020-0107-0.
37. Kikkert, M., Doolman, R., Dai, M., Avner, R., Hassink, G., van Voorden, S., Thanedar, S., Roitelman, J., Chau, V., and Wiertz, E. (2004). Human HRD1 is an E3 ubiquitin ligase involved in degradation of proteins from the endoplasmic reticulum. J. Biol. Chem. *279*, 3525–3534. https://doi.org/10.1074/jbc.M307453200.
38. Iida, Y., Fujimori, T., Okawa, K., Nagata, K., Wada, I., and Hosokawa, N. (2011). SEL1L protein critically determines the stability of the HRD1-SEL1L endoplasmic reticulum-associated degradation (ERAD) complex to optimize the degradation kinetics of ERAD substrates. J. Biol. Chem. *286*, 16929–16939. https://doi.org/10.1074/jbc.M110.215871.
39. Sun, S., Shi, G., Han, X., Francisco, A.B., Ji, Y., Mendonça, N., Liu, X., Locasale, J.W., Simpson, K.W., Duhamel, G.E., et al. (2014). Sel1L is indispensable for mammalian endoplasmic reticulum-associated degradation, endoplasmic reticulum homeostasis, and survival. Proc. Natl. Acad. Sci. USA *111*, E582–E591. https://doi.org/10.1073/pnas.1318114111.
40. Wu, X., and Rapoport, T.A. (2018). Mechanistic insights into ER-associated protein degradation. Curr. Opin. Cell Biol. *53*, 22–28. https://doi.org/10.1016/j.ceb.2018.04.004.
41. Zheng, N., and Shabek, N. (2017). Ubiquitin Ligases: Structure, Function, and Regulation. Annu. Rev. Biochem. *86*, 129–157. https://doi.org/10.1146/annurev-biochem-060815-014922.
42. Alexandru, G., Graumann, J., Smith, G.T., Kolawa, N.J., Fang, R., and Deshaies, R.J. (2008). UBXD7 binds multiple ubiquitin ligases and implicates p97 in HIF1alpha turnover. Cell *134*, 804–816. https://doi.org/10.1016/j.cell.2008.06.048.
43. Shi, W., Ding, R., Zhou, P.P., Fang, Y., Wan, R., Chen, Y., and Jin, J. (2020). Coordinated Actions Between p97 and Cullin-RING Ubiquitin Ligases for Protein Degradation. Adv. Exp. Med. Biol. *1217*, 61–78. https://doi.org/10.1007/978-981-15-1025-0_5.
44. Pan, Z.Q., Kentsis, A., Dias, D.C., Yamoah, K., and Wu, K. (2004). Nedd8 on cullin: building an expressway to protein destruction. Oncogene *23*, 1985–1997. https://doi.org/10.1038/sj.onc.1207414.
45. Markmiller, S., Fulzele, A., Higgins, R., Leonard, M., Yeo, G.W., and Bennett, E.J. (2019). Active Protein Neddylation or Ubiquitylation Is Dispensable for Stress Granule Dynamics. Cell Rep. *27*, 1356–1363.e3. https://doi.org/10.1016/j.celrep.2019.04.015.
46. Nadav, E., Shmueli, A., Barr, H., Gonen, H., Ciechanover, A., and Reiss, Y. (2003). A novel mammalian endoplasmic reticulum ubiquitin ligase homologous to the yeast Hrd1. Biochem. Biophys. Res. Commun. *303*, 91–97. https://doi.org/10.1016/s0006-291x(03)00279-1.
47. Lu, Y., Qiu, Y., Chen, P., Chang, H., Guo, L., Zhang, F., Ma, L., Zhang, C., Zheng, X., Xiao, J., et al. (2019). ER-localized Hrd1 ubiquitinates and inactivates Usp15 to promote TLR4-induced inflammation during bacterial infection. Nat. Microbiol. *4*, 2331–2346. https://doi.org/10.1038/s41564-019-0542-2.
48. Ye, Y., Shibata, Y., Kikkert, M., van Voorden, S., Wiertz, E., and Rapoport, T.A. (2005). Recruitment of the p97 ATPase and ubiquitin ligases to the site of retrotranslocation at the endoplasmic reticulum membrane. Proc. Natl. Acad. Sci. USA *102*, 14132–14138. https://doi.org/10.1073/pnas.0505006102.
49. Gauss, R., Sommer, T., and Jarosch, E. (2006). The Hrd1p ligase complex forms a linchpin between ER-lumenal substrate selection and Cdc48p recruitment. EMBO J. *25*, 1827–1835. https://doi.org/10.1038/sj.emboj.7601088.
50. Seguin, S.J., Morelli, F.F., Vinet, J., Amore, D., De Biasi, S., Poletti, A., Rubinsztein, D.C., and Carra, S. (2014). Inhibition of autophagy, lysosome and VCP function impairs stress granule assembly. Cell Death Differ. *21*, 1838–1851. https://doi.org/10.1038/cdd.2014.103.
51. Cormier, J.H., Tamura, T., Sunryd, J.C., and Hebert, D.N. (2009). EDEM1 recognition and delivery of misfolded proteins to the SEL1L-containing ERAD complex. Mol. Cell *34*, 627–633. https://doi.org/10.1016/j.molcel.2009.05.018.
52. Gao, Y., Li, Y., Zhang, C., Zhao, M., Deng, C., Lan, Q., Liu, Z., Su, N., Wang, J., Xu, F., et al. (2016). Enhanced Purification of Ubiquitinated Proteins by Engineered Tandem Hybrid Ubiquitin-binding Domains (ThUBDs). Mol. Cell. Proteomics *15*, 1381–1396. https://doi.org/10.1074/mcp.o115.051839.
53. Maxwell, B.A., Gwon, Y., Mishra, A., Peng, J., Nakamura, H., Zhang, K., Kim, H.J., and Taylor, J.P. (2021). Ubiquitination is essential for recovery of cellular activities after heat shock. Science *372*, eabc3593. https://doi.org/10.1126/science.abc3593.
54. Brodsky, J.L. (2012). Cleaning up: ER-associated degradation to the rescue. Cell *151*, 1163–1167. https://doi.org/10.1016/j.cell.2012.11.012.
55. Harding, H.P., Zhang, Y., and Ron, D. (1999). Protein translation and folding are coupled by an endoplasmic-reticulum-resident kinase. Nature *397*, 271–274. https://doi.org/10.1038/16729.
56. Lee, J.E., Cathey, P.I., Wu, H., Parker, R., and Voeltz, G.K. (2020). Endoplasmic reticulum contact sites regulate the dynamics of membraneless organelles. Science *367*, eaay7108. https://doi.org/10.1126/science.aay7108.
57. Child, J.R., Chen, Q., Reid, D.W., Jagannathan, S., and Nicchitta, C.V. (2021). Recruitment of endoplasmic reticulum-targeted and cytosolic mRNAs into membrane-associated stress granules. RNA *27*, 1241–1256. https://doi.org/10.1261/rna.078858.121.
58. Sheng, X., Xia, Z., Yang, H., and Hu, R. (2024). The ubiquitin codes in cellular stress responses. Protein Cell *15*, 157–190. https://doi.org/10.1093/procel/pwad045.
59. Jayabalan, A.K., Sanchez, A., Park, R.Y., Yoon, S.P., Kang, G.Y., Baek, J.H., Anderson, P., Kee, Y., and Ohn, T. (2016). NEDDylation promotes stress granule assembly. Nat. Commun. *7*, 12125. https://doi.org/10.1038/ncomms12125.
60. Tolay, N., and Buchberger, A. (2021). Comparative profiling of stress granule clearance reveals differential contributions of the ubiquitin system. Life Sci. Alliance *4*, e202000927. https://doi.org/10.26508/lsa.202000927.
61. El Khouri, E., Le Pavec, G., Toledano, M.B., and Delaunay-Moisan, A. (2013). RNF185 is a novel E3 ligase of endoplasmic reticulum-associated degradation (ERAD) that targets cystic fibrosis transmembrane conductance regulator (CFTR). J. Biol. Chem. *288*, 31177–31191. https://doi.org/10.1074/jbc.M113.470500.
62. van de Weijer, M.L., Krshnan, L., Liberatori, S., Guerrero, E.N., Robson-Tull, J., Hahn, L., Lebbink, R.J., Wiertz, E.J.H.J., Fischer, R., Ebner, D., and Carvalho, P. (2020). Quality Control of ER Membrane Proteins by the RNF185/Membralin Ubiquitin Ligase Complex. Mol. Cell *80*, 374–375. https://doi.org/10.1016/j.molcel.2020.09.023.
63. Hetz, C. (2012). The unfolded protein response: controlling cell fate decisions under ER stress and beyond. Nat. Rev. Mol. Cell Biol. *13*, 89–102. https://doi.org/10.1038/nrm3270.
64. Hetz, C., Zhang, K., and Kaufman, R.J. (2020). Mechanisms, regulation and functions of the unfolded protein response. Nat. Rev. Mol. Cell Biol. *21*, 421–438. https://doi.org/10.1038/s41580-020-0250-z.
65. Han, D., Lerner, A.G., Vande Walle, L., Upton, J.P., Xu, W., Hagen, A., Backes, B.J., Oakes, S.A., and Papa, F.R. (2009). IRE1alpha kinase activation modes control alternate endoribonuclease outputs to determine divergent cell fates. Cell *138*, 562–575. https://doi.org/10.1016/j.cell.2009.07.017.
66. McCormick, C., and Khaperskyy, D.A. (2017). Translation inhibition and stress granules in the antiviral immune response. Nat. Rev. Immunol. *17*, 647–660. https://doi.org/10.1038/nri.2017.63.
67. Advani, V.M., and Ivanov, P. (2020). Stress granule subtypes: an emerging link to neurodegeneration. Cell. Mol. Life Sci. *77*, 4827–4845. https://doi.org/10.1007/s00018-020-03565-0.
68. Anderson, P., Kedersha, N., and Ivanov, P. (2015). Stress granules, P-bodies and cancer. Biochim. Biophys. Acta *1849*, 861–870. https://doi.org/10.1016/j.bbagrm.2014.11.009.
69. Ma, W., and Mayr, C. (2018). A Membraneless Organelle Associated with the Endoplasmic Reticulum Enables 3′UTR-Mediated Protein-Protein Interactions. Cell *175*, 1492–1506.e19. https://doi.org/10.1016/j.cell.2018.10.007.
70. Jin, J., Li, X., Gygi, S.P., and Harper, J.W. (2007). Dual E1 activation systems for ubiquitin differentially regulate E2 enzyme charging. Nature *447*, 1135–1138. https://doi.org/10.1038/nature05902.
71. Costa, G.L., Bauer, J.C., McGowan, B., Angert, M., and Weiner, M.P. (1996). Site-directed mutagenesis using a rapid PCR-based method. Methods Mol. Biol. *57*, 239–248. https://doi.org/10.1385/0-89603-332-5:239.

STAR★METHODS

KEY RESOURCES TABLE

REAGENT or RESOURCE	SOURCE	IDENTIFIER
Antibodies		
Mouse anti-Ubiquitin(P4D1)	Cell Signaling Technology	Cat# 3936; RRID: AB_331292
Rabbit anti-K48-linkage Specific Polyubiquitin	Cell Signaling Technology	Cat# 8081; RRID: AB_10859893
Rabbit anti-K63-linkage Specific Polyubiquitin	Cell Signaling Technology	Cat# 5621; RRID: AB_10827985
Mouse anti-G3BP	Abcam	Cat# ab56574; RRID: AB_941699
Rabbit anti-G3BP1	Proteintech	Cat# 13057-2-AP; RRID: AB_2232034
Rabbit anti-TDP43	ABclonal	Cat# A1183; RRID: AB_2758796
Rabbit anti-Cullin1	Invitrogen	Cat# 71-8700; RRID: AB_2534002
Mouse anti-Vinculin	Sigma-Aldrich	Cat# V9131; RRID: AB_477629
Rabbit anti-β-Actin	ABclonal	Cat# AC026; RRID: AB_2768234
Mouse anti-GFP	ABclonal	Cat# AE012; RRID: AB_2770402
Mouse anti-Flag	Sigma-Aldrich	Cat# F3165; RRID: AB_259529
Rabbit anti-HRD1	Proteintech	Cat# 13473-1-AP; RRID: AB_2287023
Rabbit anti-SEL1L	ABclonal	Cat# A12073; RRID: AB_2758977
Rabbit anti-VCP	Bethyl Laboratories	Cat# A300-589A; RRID: AB_495512
Mouse anti-VCP	Invitrogen	Cat# MA3-004; RRID: AB_2214638
Rabbit anti-PERK	Cell Signaling Technology	Cat# 5683; RRID: AB_10841299
Rabbit anti-p-eIF2α(Ser51)	Cell Signaling Technology	Cat# 3398; RRID: AB_2096481
Rabbit anti-eIF2α	ABclonal	Cat# A0764; RRID: AB_2757387
Rabbit anti-p-IRE1α(Ser724)	Genetex	Cat# gtx63722; RRID: AB_3101842
Rabbit anti-IRE1α	Cell Signaling Technology	Cat# 3294; RRID: AB_823545
Rabbit anti-XBP1s	Cell Signaling Technology	Cat# 12782; RRID: AB_2687943
Rabbit anti-ATF6	Proteintech	Cat# 24169-1-AP; RRID: AB_2876891
Rabbit anti-BiP	Cell Signaling Technology	Cat# 3177; RRID: AB_2119845
Chemicals, peptides, and recombinant proteins		
$NaAsO_2$	Sigma-Aldrich	Cat# S7400
Sorbitol	Sigma-Aldrich	Cat# S1876
H_2O_2	Sigma-Aldrich	Cat# 323381
TAK-243	MedChemExpress	Cat# HY-100487
CB-5083	ApexBio	Cat# B6032
Bortezomib	ApexBio	Cat# A2614
MLN4924	Boston BioChem	Cat# I502-01M
LS-102	MedChemExpress	Cat# HY-135844
Tunicamycin	Cell Signaling Technology	Cat# 12819
GSK2606414	MedChemExpress	Cat# HY-18072
Salubrinal	MedChemExpress	Cat# HY-15486
Kira6	Selleck	Cat# S8658
Paraformaldehyde (PFA)	Sigma-Aldrich	Cat# P6148
Critical commercial assays		
Superscript III cDNA synthesis kit	Invitrogen	Cat# 18080051
Lipofectamine RNAiMax	Thermo Fisher Scientific	Cat# 13778075

(*Continued on next page*)

Continued

REAGENT or RESOURCE	SOURCE	IDENTIFIER
BCA protein assay kit	Thermo Fisher Scientific	Cat# 23227
ER-Tracker™ Red (BODIPY™ TR Glibenclamide)	Invitrogen	Cat# E34250
T4 DNA ligase	New England Biolabs	Cat# M0202L
Phusion high-fidelity DNA polymerase	New England Biolabs	Cat# M0530S
LR Clonase	Invitrogen	Cat# 11791020
anti-Flag beads	Millipore	Cat# A2220
ProLong Gold Antifade reagent with DAPI	Invitrogen	Cat# P36935
Experimental models: Cell lines		
U2OS	ATCC	Cat# HTB-96
HeLa	ATCC	Cat# CRM-CCL-2
HEK293T	ATCC	Cat# CRL-11268
HeLa-EGFP-G3BP1	This study	N/A
U2OS-EGFP-G3BP1	This study	N/A
U2OS-EGFP-G3BP1& HRD1-Flag-strep-rescue	This study	N/A
U2OS-EGFP-G3BP1& HRD1-ΔN-Flag-strep-rescue	This study	N/A
U2OS-EGFP-G3BP1& HRD1-C329A-Flag-strep-rescue	This study	N/A
U2OS-EGFP-G3BP1& SEL1L-Flag-strep-rescue	This study	N/A
U2OS-EGFP-G3BP1& Flag-strep-eIF2α-rescue	This study	N/A
U2OS-EGFP-G3BP1& Flag-strep-eIF2α-S51A-rescue	This study	N/A
Oligonucleotides		
siCtrl (CGUACGCGGAAUACUUCGA[dT][dT])	Sunya (Hangzhou, China)	N/A
siATF6 (GCAGCAACCAAUUAUCAGUUU[dT][dT])	Sunya (Hangzhou, China)	N/A
siBiP (GGAGCGCAUUGAUACUAGU[dT][dT])	Sunya (Hangzhou, China)	N/A
sieIF2α (GGCUUGUUAUGGUUAUGAA[dT][dT])	Sunya (Hangzhou, China)	N/A
siHRD1 (UCAUCAAGGUUCUGCUGUA[dT][dT])	Sunya (Hangzhou, China)	N/A
siIRE1α (AAGAUGGACUGGCGGGAGA[dT][dT])	Sunya (Hangzhou, China)	N/A
siPERK (UAGCAAAUCUUCUUCUGAA[dT][dT])	Sunya (Hangzhou, China)	N/A
siSEL1L (GCCUCUGGACUUGGUGUUAAU[dT][dT])	Sunya (Hangzhou, China)	N/A
siRNA oligos used in siRNA screen	See Table S1 for detailed information	N/A
Recombinant DNA		
pHAGE-PGK-N-EGFP-G3BP1-IRES-Puro	This study	N/A
pHAGE-PGK-HRD1-Rescue-C-Flag-strep-IRES-Blast	This study	N/A
pHAGE-PGK-HRD1-ΔN-Rescue-C-Flag-strep-IRES-Blast	This study	N/A
pHAGE-PGK-HRD1-C329A-Rescue-C-Flag-strep-IRES-Blast	This study	N/A
pHAGE-PGK-SEL1L-Rescue-C-Flag-strep-IRES-Blast	This study	N/A
pHAGE-PGK-N-Flag-Strep-eIF2α-Rescue-IRES-Blast	This study	N/A
pHAGE-PGK-N-Flag-Strep-eIF2α-S51A-Rescue-IRES-Blast	This study	N/A
pcDNA-mCherry-SEC61B	Ma and Mayr[69]	N/A
pcDNA3.0-BiP-3xFlag-KDEL	This study	N/A
pcDNA3.1	Addgene	Cat# V79020
Software and algorithms		
Image J	N/A	https://imagej.nih.gov/ij/
GraphPad Prism 9.0	GraphPad Software	https://www.graphpad.com/

RESOURCE AVAILABILITY

Lead contact

Further information and requests for resources and reagents should be directed to and will be fulfilled by the lead contact: Jianping Jin (jianping_jin@zju.edu.cn).

Materials availability

All materials in this study are available from the lead contact on request.

Data and code availability

- All data reported in this paper will be shared by the lead contact upon reasonable request.
- This paper does not report original code.
- Any additional information reported in this paper is available from the lead contact upon request.

EXPERIMENTAL MODEL AND STUDY PARTICIPANT DETAILS

Cell culture

HEK293T, HeLa, U2OS cells and the related stable cell lines were cultured in DMEM (Dulbecco's modified Eagle's medium, Gibco) supplemented with 10% fetal bovine serum. Cells were maintained in a humidified incubator at 37°C with 5% CO_2 to ensure proper growth conditions.

METHOD DETAILS

Establishing stable cell lines

The indicated HeLa and U2OS stable cell lines in key resources table were generated using a lentivirus expression system. The experimental procedures of lentivirus production and infection were previously described.[70] The expression levels and localizations of the ectopic proteins were validated by Western blot and immunofluorescence after proper antibiotic selection to get rid of uninfected cells.

Plasmid construction

Plasmids were constructed using the Gateway LR cloning system except for pcDNA3.0-BiP-3xFlag-KDEL. For human G3BP1, HRD1, SEL1L, their coding sequences (CDS) were PCR-amplified using the Phusion high-fidelity DNA polymerase from HeLa cDNAs library that was generated by a Superscript III cDNA synthesis kit, and the PCR products were subsequently subcloned into the Gateway entry vector using T4 DNA ligase. Gateway entry clones containing CDS of human HRD1 and eIF2α were obtained from Ultimate™ ORF LITE Clones (Human collection, Invitrogen), and maintained by the Core Facility of Life Sciences Institute, Zhejiang University. All plasmids' constructs were verified by nucleic acid sequencing. After verification, the entry clones were shuttled to Gateway destination vectors containing either EGFP or Flag-strep tag using the LR Clonase. The siRNA-resistant wildtype or mutant rescue plasmids were generated using a PCR-based mutagenesis method according to published method.[71]

RNA interference

siRNA knockdown experiments were performed using Lipofectamine RNAiMax according to the manufacturer's protocol.

For siRNA screening of ubiquitin ligases, candidates are mainly selected from reported G3BP1 or p97 associated non-cullin RING ubiquitin ligases by searching BioGRID (https://thebiogrid.org/) or refer to a previous study.[42] Each candidate gene was designed to have two siRNA oligos and their corresponding sequences are listed in Table S1.

SG assembly/disassembly and chemicals treatments

For the heat shock induced-SG assembly, the standard culture medium was aspirated and replaced with medium pre-warmed up to 43°C. Then cells were transferred to a 43°C humidified incubator with 5% CO_2 immediately for indicated incubation times. For the heat shock-induced SG disassembly, right after heat shock treatment for 30 minutes, cells were transferred back to a regular 37°C incubator to allow for recovery at indicated times. For the arsenite-induced SG assembly, $NaAsO_2$ dissolved in sterile water was added to cells at a working concentration of 0.5 mM for indicated times. For the arsenite-stimulated SG disassembly, $NaAsO_2$ was added to cells at the working concentration of 0.5 mM for 30 minutes, and then the medium was aspirated and washed with pre-warmed 37°C PBS for once and replaced with pre-warmed 37°C standard medium for recovery at indicated times.

Chemicals were dissolved in DMSO and added to cells 15 minutes prior to either SG assembly induced by heat shock or arsenite, or disassembly at the following concentrations: TAK-243 (5 μM), CB-5083 (10 μM) and Bortezomib (10 μM). MLN4924 (10 μM), LS-102 (5 μM), Tunicamycin (20 μM), GSK2606414 (1 μM), Salubrinal (20 μM), Kira6 (5 μM).

Western blot

For western blot, cells were collected and washed with iced cold PBS using centrifugation at 4°C. Cell pellets were then lysed in an SDS lysis buffer (1% SDS, 30mM Tris-HCl, pH6.8) by heating samples at 95°C for 10 minutes twice. The lysate was then cleared by ultracentrifugation briefly at room temperature and quantified using a BCA protein assay kit. 10 μg lysate for each sample was loaded and separated in SDS-Polyacrylamide gels (SDS-PAGE) and then transferred onto the PVDF membrane (Millipore, IPVH00010) for detection using indicated antibodies. The primary antibodies employed in this study are listed in the key resources table. Mouse and rabbit HRP-conjugated secondary antibodies for western blot were purchased from Jackson ImmunoResearch (115-035-003 and 111-035-003 respectively).

Co-Immunoprecipitation (co-IP)

For co-IP experiments, cells were washed with pre-warmed 43°C PBS and harvested on a pre-warmed 43°C dry bath. Cell pellets were then lysed in a 1% Trion lysis buffer (1% Trion X-100, 50 mM Tris-HCl, pH7.5, 150 mM NaCl, 1mM EDTA, and freshly added 10 mM β-glycerol phosphate, 10 mM p-nitrophenyl phosphate, 0.1 mM okadaic acid, 5 μg/ml aprotinin, 1 μg/ml pepstatin, 1 mM leupeptin, 0.1 mM phenylmethylsulphonyl fluoride, and 0.5mM N-Ethylmaleimide [NEM]), and the lysate was cleared by ultracentrifugation at 4°C for 10 minutes. The extract was incubated with anti-Flag beads at 4°C for 2.5 hours with slow rotation. Unbound proteins were washed away using the extraction buffer for four times, and bead-bound proteins were then eluted with SDS-PAGE loading buffer (50 mM Tris–HCl pH 6.8, 2% SDS, 0.1% bromophenol blue, 10% glycerol, and 2% 2-Mercaptoethanol) by heating at 95°C for 5 minutes, the eluent was loaded and separated in SDS-PAGE, followed by immunoblotting using indicated antibodies.

Immunofluorescence and microscopic imaging

For immunofluorescence, cells were grown on a coverslip and treated at 43°C for 30 minutes when the cells reached about 70% confluency. The culture medium was aspirated and cells were fixed using pre-warmed (43°C) 4% paraformaldehyde (PFA) in PBS for 5 min at 43°C immediately. Cells were then washed with PBS for three times, followed by permeabilization using 0.2% Triton X-100 in PBS for 10 minutes, and blocking using PBS containing 3% BSA and 0.1% Tween 20 for 30 minutes at room temperature. Samples were then incubated with indicated primary antibodies in PBS containing 1% BSA and 0.1% Tween 20 at 4°C for overnight. After PBST washing for three times, samples were then incubated with host-specific Alexa Fluor 488/546 secondary antibodies (Invitrogen; A11029, A11035) for 1 hour at room temperature, followed by washing with PBST and subsequent PBS for twice. The coverslips were prepared for microscopic imaging by mounting them with ProLong Gold Antifade reagent with DAPI, and images were captured using a Zeiss LSM880 confocal microscope with a 63x oil-immersion objective lens.

For ER and SG co-staining, U2OS cells stably expressing EGFP-G3BP1 were seeded on coverslips. When cells reached to about 70% confluency, the ER was stained using 0.75 μM ER Tracker for 15 minutes and replaced with pre-warmed 43°C culture medium containing 0.75 μM ER Tracker to incubate for an additional 30 minutes. After the heat shock treatment, the cells were fixed with pre-warmed 43°C 4% PFA in PBS for 5 min at 43°C immediately, followed by washing with PBS for three times. The coverslips were prepared for microscopic imaging with the mounting medium mentioned above, and the images were captured by the CSU-W1 Sora module of Olympus IXplore SpinSR confocal microscope, with a 63x oil-immersion objective lens. Alternatively, U2OS cells stably expressing EGFP-G3BP1 were seeded on coverslip and the mCherry-tagged ER marker, mCherry-Sec61B was transiently introduced into cells using the plasmid transfection approach. Cells were subjected to heat shock treatment and fixed. The slides were prepared by the same way described above. Images were captured using the Airyscan module of Zeiss LSM880 confocal microscope with a 63x oil-immersion objective lens.

QUANTIFICATION AND STATISTICAL ANALYSIS

For SG assembly and disassembly statistical analysis, U2OS cells stably expressing EGFP-G3BP1 seeded on coverslips were subjected to heat shock or arsenite treatment as described above for indicated times, and fixed using pre-warmed (43°C or 37°C) 4% PFA respectively. Images were captured using Olympus CKX53 wide-field fluorescence microscope with a 63x oil-immersion objective lens. The size and number of SGs were measured in ImageJ using the analyze particle function with particle size and circularity parameters fixed. Cells harboring SGs were manually counted according to the microscopic visible EGFP-G3BP1 foci. Any cells with more than 3 distinct foci were considered as stress granule positive. Unless otherwise indicated, all the quantification data of cells with SGs are shown as the mean ± SD from $n = 3$ replicates, with >450 cells per condition. Statistical analysis was performed using GraphPad Prism. The normal distribution of the all the quantification data was verified by performing the D'Agostino & Pearson test or Shapiro–Wilk test using Normality and Lognormality Tests in GraphPad. Comparisons between two means were determined using unpaired, two-tailed Student's t tests; Comparisons among multiple means were performed using one-way ANOVA with a Tukey's multiple comparisons test; For group comparation, two-way ANOVA with a Sidak's multiple comparisons test was employed. The following p-values were considered significant: *=$p \leq 0.05$; **=$p \leq 0.01$; ***=$p \leq 0.001$; ****= $p \leq 0.0001$, ns means no significant.